Journal of Applied Physics

Molecular and thermodynamics descriptions of flow-induced crystallization in semi-crystalline polymers

Cite as: J. Appl. Phys. **127**, 241101 (2020); https://doi.org/10.1063/5.0012376
Submitted: 30 April 2020 • Accepted: 04 June 2020 • Published Online: 22 June 2020

Wei Chen, Qianlei Zhang, Jingyun Zhao, et al.

Journal of Applied Physics TUTORIAL scitation.org/journal/jap

Molecular and thermodynamics descriptions of flow-induced crystallization in semi-crystalline polymers

Cite as: J. Appl. Phys. **127**, 241101 (2020); doi: 10.1063/5.0012376
Submitted: 30 April 2020 · Accepted: 4 June 2020 ·
Published Online: 22 June 2020

Wei Chen, Qianlei Zhang, Jingyun Zhao, and Liangbin Li[a)]

AFFILIATIONS

National Synchrotron Radiation Laboratory, Anhui Provincial Engineering Laboratory of Advanced Functional Polymer Film, CAS Key Laboratory of Soft Matter Chemistry, University of Science and Technology of China, Hefei 230026, China

[a)]**Author to whom correspondence should be addressed:** lbli@ustc.edu.cn

ABSTRACT

The flow-induced crystallization (FIC) is commonly encountered in the polymer industry as more than 70% of commercial polymers are crystalline, which needs to be processed before the final application. The complicated external flow field, i.e., shear or extensional flow, results in a great challenge in understanding the FIC phenomenon from both general thermodynamics and detailed molecular level aspects. The current tutorial first describes the general phenomenon of FIC from the aspect of different morphologies and enhanced kinetics induced by the flow. Second, characterization methods for monitoring FIC are introduced. Here, the *in situ* synchrotron x-ray scattering and non-equilibrium molecular dynamics simulation are selected as typical examples. Then, the theoretical descriptions of FIC are summarized from the aspects of molecular origin and thermodynamics. The coil–stretch transition theory and later developed stretched network theory are highlighted, where the former mainly accounts for polymer dilute solution and the latter for highly entangled cases. Also, multistep features for the formation of various intermediate states during flow-induced nucleation are depicted. Despite non-equilibrium nature, the FIC can still be treated by thermodynamics, especially under weak flow conditions. The classic entropy reduction model is introduced together with later modifications. In all, understanding the fundamental mechanism of FIC is crucial for optimizing external processing parameters and internal molecular characteristics, and useful to guide current or further applied techniques.

I. INTRODUCTION

Semicrystalline polymers are the most widely used polymeric materials, and polyethylene (PE) and polypropylene (PP) together accounted for 57% of all synthetic polymers.[1] Almost all semicrystalline polymers need to be processed from the initial melt state to the final semicrystalline state, where the processing condition plays a central role. Since the properties of final products are closely related to the final structure, which is significantly influenced by processing, researchers and engineers try to establish the processing–structure–property relationship. Concerning processing conditions, flow and temperature are the most important parameters. The influence of temperature on the crystallization behavior of semicrystalline polymers has been extensively explored ever since the early investigation of polymer crystallization. Most conclusions are obtained in quiescent conditions. Readers interested in such topics are suggested to other reviews or books.[2–10] The polymer crystallization influenced by flow, namely, flow-induced crystallization (FIC), will be discussed in the current work.

In industry, various processing techniques, i.e., melt-spinning, film casting, film blowing, and injection molding, are used to obtain different products meeting different application requirements. During these processes, the external flow is found to significantly enhance the crystallization kinetics and generate oriented crystallites. Both phenomena are closely related to nuclei density and oriented crystallite (point-like[11] and oriented[12] ones as shown in Fig. 1). Therefore, most research studies in FIC attempt to couple the external flow parameters (e.g., shearing rate and time) with final crystal morphology. However, different from quiescent crystallization, the FIC is far away from the equilibrium state, and the flow is always complicated in the real application, i.e., multidimensional and non-uniform, resulting in a great challenge in capturing the *in situ* microstructure evolution under flow.

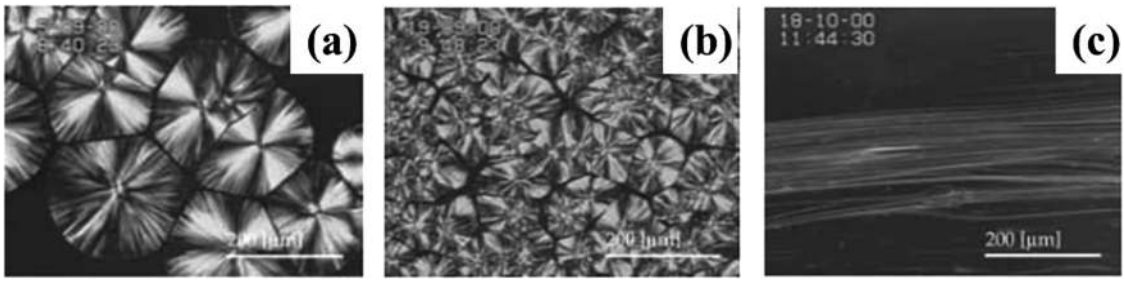

FIG. 1. Crystal morphology (T = 135 °C) of *i*-PP obtained under (a) quiescent condition, and after shearing with a strain rate of 60 (s^{-1}) for the shearing time of (b) 1 s and (c) 6 s. Reproduced with permission from Housmans *et al.*, J. Therm. Anal. Calorim. **98**(3), 693–705 (2009). Copyright 2009 Springer Nature.

Despite external flow conditions, the semicrystalline polymer is also intrinsically complicated compared with a small molecule. The long-chain nature of polymer results in much longer relaxation time as compare with normal Newton fluids.[13] As a result, the processing flow can significantly distort local chain conformation leading to the anisotropic feature of the polymer melt.[14] Later on, the anisotropic melt suffering from cooling starts to transform into the semicrystalline state, where crystallization and chain relaxation start to compete with each other.[15] Therefore, both the rheological behavior of the polymer melt and microstructure evolution under flow are crucial to understand the FIC phenomenon. However, several molecular characteristics of the polymer, i.e., polydispersity and branched architecture, severely complicate the analysis of experimental data and final establishment of the process–structure–property relationship.

As a tutorial, we aim to present the basic issues of FIC in the semicrystalline polymer system. The detailed historical summary of FIC is far beyond the scope of the current tutorial. The current tutorial is organized as follows. In Sec. II, the general phenomenon of FIC is presented including oriented crystallite and enhanced crystallization kinetics induced by the flow. So readers can get a general idea of FIC. In Sec. III, we present methods for observing FIC. Here, the synchrotron radiation x-ray scattering and non-equilibrium molecular dynamic simulation are discussed in detail. In Sec. IV, the theories accounting for the formation of different crystal morphologies are presented. The coil–stretch transition (CST) theory and later developed stretched network model are discussed in detail. These two theories together with their modifications can well explain the morphology formation under flow from dilute solution to high concentrated and melt states. In Sec. V, the thermodynamics treatment of FIC is presented. Although FIC is a typical non-equilibrium process, the FIC can be still dealt with by conventional thermodynamics concepts, i.e., Gibbs free energy, to present a thermodynamics phenomenological image, especially under a weak flow condition. The thermodynamics treatment can qualitatively or sometimes even quantitatively reproduce the enhanced crystallization kinetics. Finally, the key features together with our perspectives of FIC are presented.

II. PHENOMENON OF FIC

A. Shear and extensional flow

The flow is inevitable in the real processing of polymers. Before further addressing the influence of flow on polymer crystallization, the definition and classification of different flow fields are briefly discussed. Figure 2(a) shows the inner structure of an extruder. The extrusion is commonly the very first step before any further processing of a polymer. The flow field, as shown in Fig. 2(b), is quite complicated. However, such complicated flow can be decomposed into two basic flows: the shear flow [Fig. 2(c)] and extension one [Fig. 2(d)]. An apparent characteristic of the shear flow is the velocity gradient. For the extension flow, the strain rate is the same for different positions along the vertical direction. Since the flow is crucial for FIC, the key parameters, i.e., the strain rate and strain, have been extensively studied. Most of the research studies related to FIC adopts one flow field to investigate the influence of different processing parameters on final crystal morphology and crystallization kinetics.

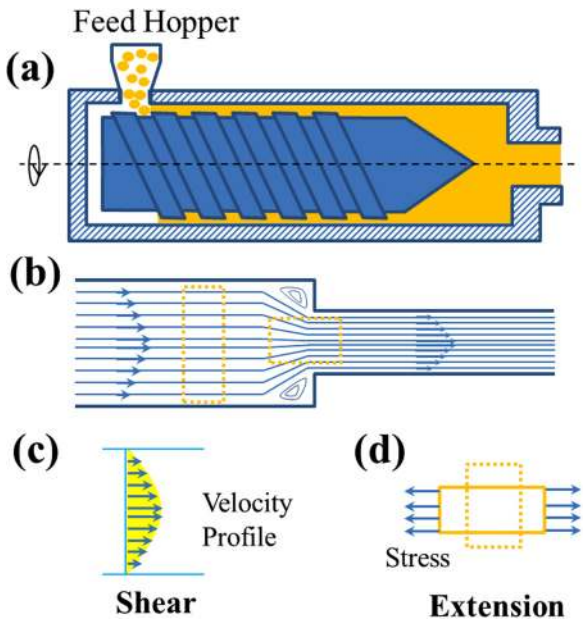

FIG. 2. (a) Schematic illustration of the extruder for polymer processing. (b) The flow field during the extrusion of the polymer melt, where both (c) shear and (d) extension flow coexist.

B. Crystal morphology

The crystal morphology in FIC has already shown in Fig. 1, where both point-like and shish–kebab structures could be formed. Since the finding of the "shish–kebab" structure initiated the research of FIC, we will first summarize the state-of-the-art understanding of the formation of the shish–kebab structure.

As shown in Fig. 3, the extended chain formed the shish core, whereas the polymer lamellae or kebab is normal to the extended shish.[16] The lamellae could twist under the low-stress condition as it did in normal polymer spherulite,[16,17] while such twist is largely suppressed under large stress. Also for kebab, there are two different kinds of kebab, namely, macro-kebab and micro-kebab.[18] The macro-kebab can be removed away from the shish through the addition of a solvent or increasing the temperature, while the micro-one remains alive within the shish. Therefore, the micro-kebab is thought to be as stable as the shish core. The micro-kebab is proposed to be inside the macro-shish and perpendicular to the macro-shish [Figs. 3(a)–3(c)]. After the discovery of the shish–kebab structure, researchers proposed various theories and models to explain the formation of this shish–kebab structure. Pioneers such as Penning,[19,20] Hoffman,[21] and Petermann and Keller[22,23] have contributed to the understanding of the nucleation and growth of the shish core. Detailed summary and comparison of relevant research studies are referred to a recent review.[24]

The flow does not necessarily lead to the formation of a shish structure. As shown in Fig. 4, the crystal morphology and crystallization kinetics (t/t_Q, t_Q is the half-time of crystallization under quiescent condition) are determined by the external flow parameters

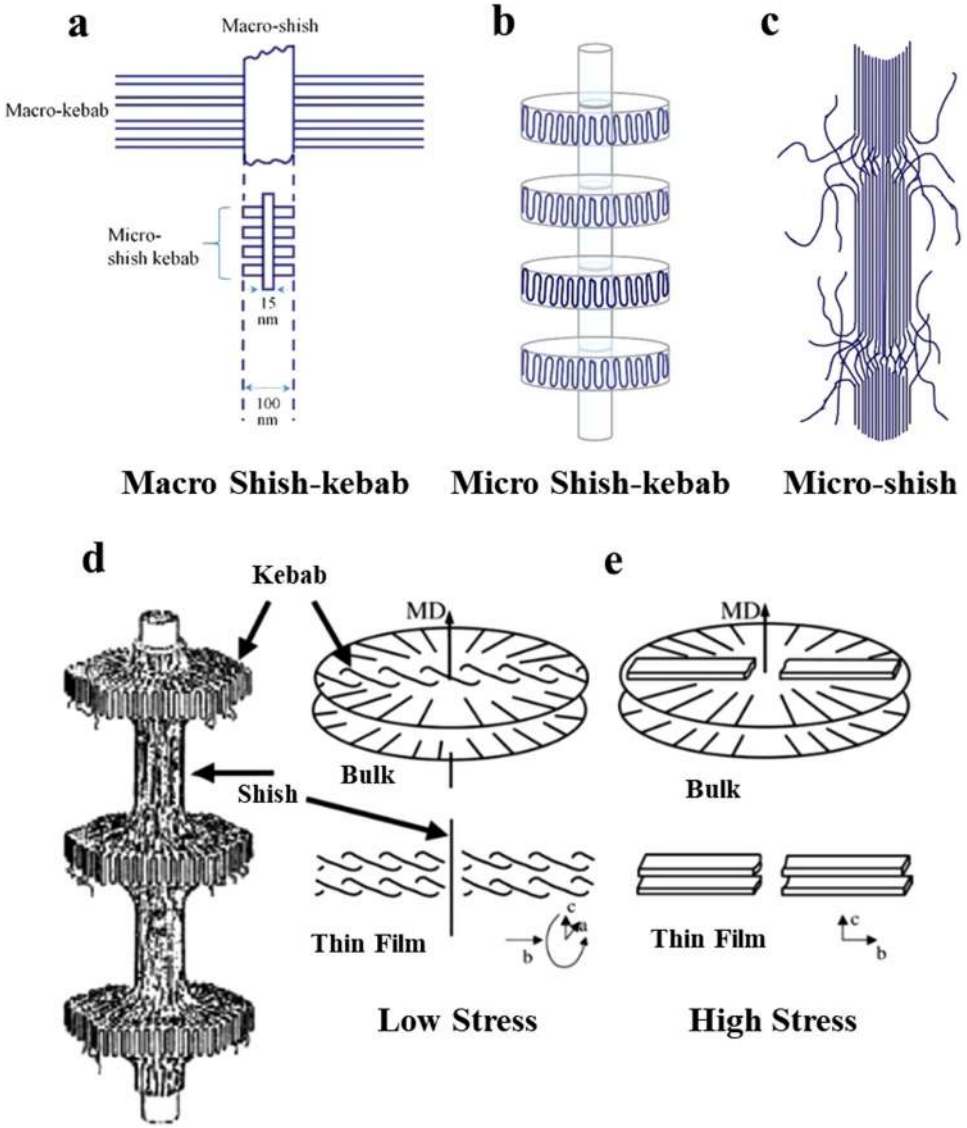

FIG. 3. Schematic illustration of (a)–(c) the macro- and micro-shish–kebab structure, together with the detailed PE shish–kebab structure under different stresses. Reproduced with permission from Keller and Kolnaar, *Materials Science and Technology*. Copyright 2006 John Wiley and Sons.

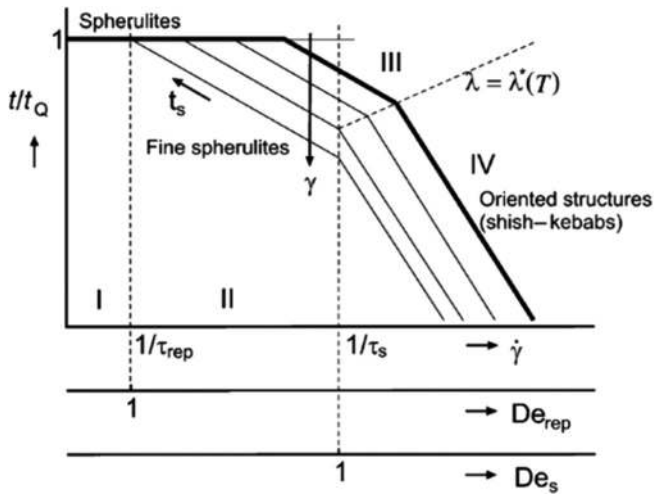

FIG. 4. The crystal morphology and crystallization kinetics evolution in different flow regimes. Reproduced with permission from Housmans *et al.*, J. Therm. Anal. Calorim. **98**(3), 693–705 (2009). Copyright 2009 Springer Nature.

(shear/strain rate $\dot{\gamma}$, strain time t_s, and strain γ) and intrinsic molecular parameters (reptation time τ_{rep} and Rouse time τ_s).[25] The boundary between two neighboring regimes is defined by rheological parameters, Deborah number, D_e, or Weissenberg number, $\mathrm{Wi} = \dot{\gamma}\tau$. De_{rep} and De_s represent chain orientation and chain stretch. In regime I ($De_{rep} < 1$ and $De_s < 1$), the polymer chains remain in the coil state. As a result, the crystal morphology keeps spherulite, and the crystallization kinetics is the same as that in the quiescent condition. In regime II ($De_{rep} > 1$ and $De_s < 1$), the whole chain starts to be orientated while the local chain conformation is not stretched. The enhanced crystallization kinetics appears ($t/t_Q < 1$), but the general crystal morphology is still spherulite. In regimes III and IV ($De_{rep} > 1$ and $De_s > 1$), the chain starts to be stretched. Despite enhanced crystallization kinetics ($t/t_Q < 1$), the shish structure appears. The prerequisite for the formation of the shish structure, or the classification of regimes III and IV, is the temperature dependence of the strain λ (T). This is because sufficient strain needs to be satisfied to generate shish, which is extensively confirmed by experiments and modeling.[26–28] Admittedly, the criteria of different regimes are not strictly represented by D_e, namely, $D_e = 1$, as mentioned above. The D_e used here mostly represents the relative difference between the external flow rate and the internal relaxation rate.

C. Enhanced crystallization kinetics

Besides the crystal morphology, another apparent change is the flow-enhanced crystallization kinetics compared with that of quiescent crystallization. Taking *i*-PP as an example, the half crystallization time decreases by the orders of magnitude due to the flow as shown in Fig. 5(a).[29] The crystallization kinetics is independent of the shear rate and shearing time.[31] Such enhanced crystallization kinetics is mainly attributed to the significantly increased nucleus density and growth rate. Figure 5(b) shows the influence of the shear rate on the nucleation rate. Compared with that in quiescent crystallization, the nucleation rate can be increased up to two orders of magnitude.[30] Such an increase seems to follow the exponential function. The flow would eventually lead to an increasing nucleation rate once the flow rate exceeds a critical value. For example, for *i*-PP ($M_w = 55\,600$, $M_n = 376\,000$, and tacticity = 87.6%), the critical shear rate is 0.048 s^{-1} ($T = 140$ °C).[32]

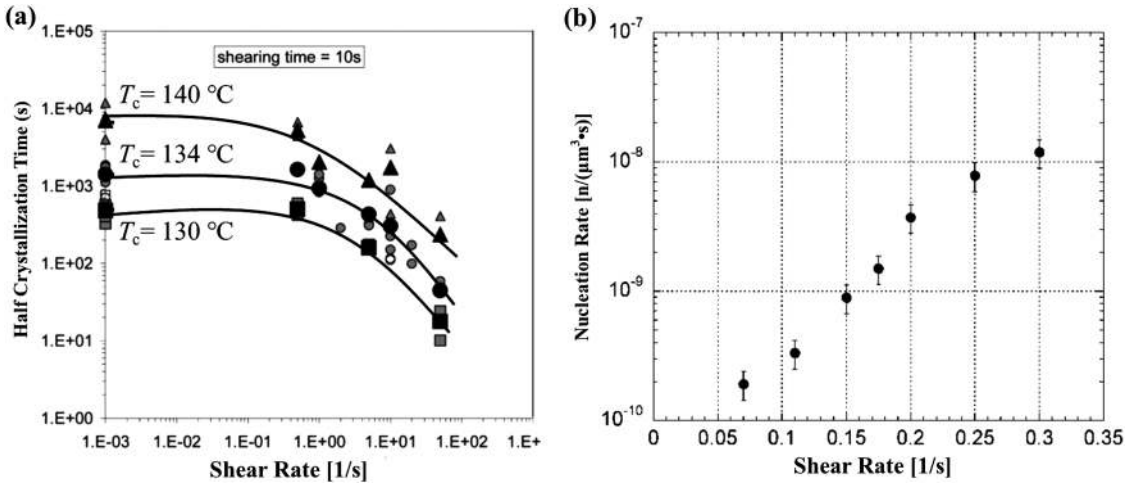

FIG. 5. (a) The half crystallization time of *i*-PP as a function of shear rate with a fixed shearing time of 10 s, where three temperatures are selected (140, 134, and 130 °C). Adapted with permission from Koscher *et al.*, Polymer **43**(25), 6931–6942 (2002). Copyright 2002 Elsevier. (b) The dependence of shear rate on the nucleation rate as obtained by the combination of Linkam shear stage and optical microscopy. Reproduced with permission from Coccorullo *et al.*, Macromolecules **41**(23), 9214–9223 (2008). Copyright 2008 American Chemical Society.

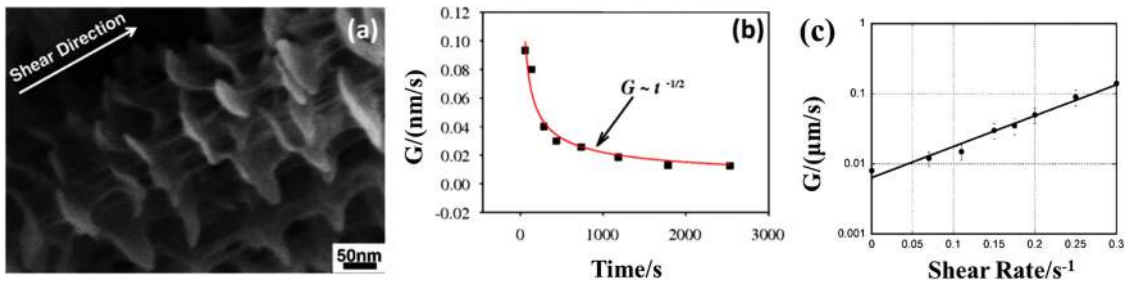

FIG. 6. (a) The multiple-shish structure as captured by scanning electron microscopy (SEM); (b) the growth rate of kebab. Adapted with permission from Hsiao *et al.*, Phys. Rev. Lett. **94**(11), 117802 (2005). Copyright 2005 American Physical Society. (c) The lateral growth rate as a function of shear rate. Reproduced with permission from Coccorullo *et al.*, Macromolecules **41**(23), 9214–9223 (2008). Copyright 2008 American Chemical Society.

In addition to increased nucleation density, the later growth is also significantly different from that in a quiescent condition. As shown in Fig. 6(a), the multiple-shish, rather than single shish, is observed in PE blends, where 2 wt. % is the ultra-high-molecular-weight PE (UHMWPE) and the remaining is the non-crystalline PE matrix.[33] With the presence of this multiple-shish, the growth rate of kebab, or more precisely, the diameter of the kebab, can be obtained by *in situ* SAXS measurement as shown in Fig. 6(b). The calculated growth rate as a function of time can be fitted by the diffusion-controlled model [$G(t) \sim t^{-1/2}$]. Such a conclusion is different from that in quiescent conditions, where the growth rate in the secondary nucleation theory is constant. This phenomenon is well consistent with the AFM[34–36] and simulation results.[37] More detailed experimental result related to the growth is shown in Fig. 6(c), where increasing shear rate up to 0.3 s^{-1} results in one order enhanced growth rate.[30]

D. Polymorphism induced by flow

The polymorphism is a common phenomenon for the semicrystalline polymer. Even for the simplest PE, at least three crystalline phases exist: orthorhombic, monoclinic, and hexagonal phases. Since the macroscopic performance of polymer products is closely related to the crystal structure,[39] an apparent question is how the external flow would influence the polymorphism. Compared with crystallization at quiescent conditions, the FIC happens far from the equilibrium state. As a result, the kinetics favored, rather than thermal stable crystalline phases could be obtained. Taking *i*-PP as an example,[38] as shown in Fig. 7(a), the non-equilibrium phase diagram of *i*-PP is obtained with the assistance of ultra-fast x-ray scattering technique. Since all experiments were conducted well above the melting temperature of both crystals, such results suggest that the strong flow can reverse the thermal stability of crystals and melts. For *i*-PP, there are numerous crystal structures, such as α, β, γ, and mesomorphic phases, whose helix conformation is 3_1. Despite the same helix conformation, different phases take different packing structures. And among all phases, the α crystal is the most thermally stable. However, with increasing strain rate and temperature, the content of the metastable β crystal also increases. The β crystal is thought to be a kinetically favored phase under a strong flow. A similar phenomenon is also observed in other semicrystalline polymer systems, i.e., poly(1-butene)[40] and PE.[41] These results suggest that the competition between thermodynamics stability and crystallization kinetics dominates the non-equilibrium phase diagram under flow. This structural information could provide roadmaps for obtaining polymer products with desired properties through tuning flow parameters.

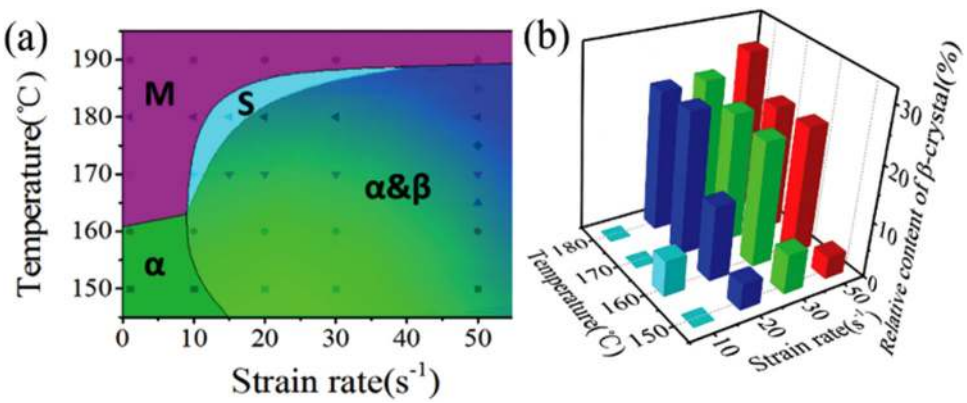

FIG. 7. (a) The non-equilibrium phase diagram of *i*-PP in strain rate–temperature space. M represents melt state, and S represents shish formation. (b) The relative content of the metastable β crystal in strain rate–temperature space. Reproduced with permission from Ju *et al.*, Macromol. Rapid Commun. **37**(17), 1441–1445 (2016). Copyright 2016 John Wiley and Sons.

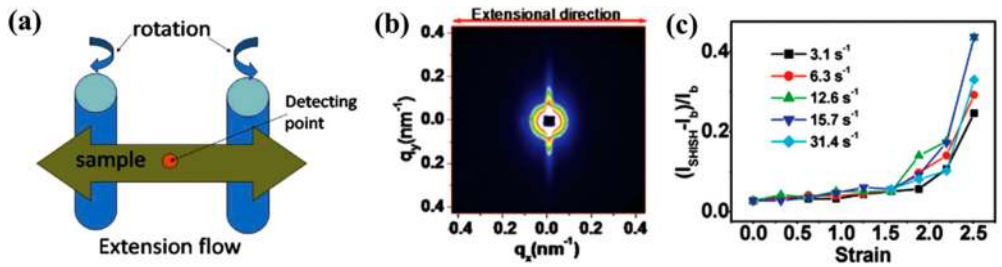

FIG. 8. (a) Schematic illustration of the setup of the extensional rheometer installed in the synchrotron x-ray beamline. (b) 2D SAXS pattern. The extensional direction is indicated. (c) The shish content as a function of strain under different strain rates. Reproduced with permission from Yan *et al.*, Macromolecules **43**(2), 602–605 (2010). Copyright 2010 American Chemical Society.

III. METHODS FOR OBSERVING FIC

The *ex situ* studies of the FIC are the mainstream during the last century, and even up to date, this strategy still has great vitality. Experimental evidence, including the crystal structure and morphology, are crucial to the understanding of the FIC by retracing the FIC process. This strategy is applicable in general polymer crystallization research.[7] However, the *in situ* observation of FIC is preferred, which can provide direct evidence of micro-structural information during FIC. With the fast development in characterization techniques in the last two decades, the *in situ* characterization of FIC from the polymer melt to the final crystalline state becomes possible. Techniques, such as rheo-AFM,[34] rheo-X-ray,[33,42] rheo-IR,[43] and rheo-Optics,[14,44] have been successfully utilized to track the microstructure evolution during FIC, especially the initial part. Also, the development of both hardware and software in molecular dynamics (MD) simulation provides a great opportunity for us to track FIC at the molecular level. Here, the x-ray scattering based on the synchrotron radiation facility and MD simulation is selected as typical examples to show current efforts to elucidate the detailed molecular origins of FIC.

A. *In situ* x-ray scattering

With the fast development of synchrotron radiation facility, the extremely high brilliance ensures the microstructure characterization of FIC with both high spatial (<100 nm) and time resolution (<1 ms). For the collection of most recent achievements in applying synchrotron radiation x-ray scattering (SRXS) in the investigation of FIC, readers are referred to other reviews.[12,45] Here, the selected examples mainly related to the setup of the experiment are shown below.

1. Extensional flow

Figure 8(a) shows the extensional rheometer commonly coupled with synchrotron radiation x-ray scattering for *in situ* measurement.[46–48]The strain rate is controlled by the rotational rate of two rotational clamps, which rotate oppositely. Since the positions of these two clamps are fixed, the sample cavity is fixed, which ensures high flow homogeneity. Figure 8(b) shows a typical 2D SAXS pattern of high-density PE (HDPE) at a strain of 2.5 (strain rate is 15.7 s^{-1}, $T = 125$ °C). The two streaks appear perpendicular to the extensional direction are assigned to the shish structure. Therefore, the formation of the shish core can be *in situ* captured by SR-SAXS as summarized in Fig. 8(c). It shows that the shish structure can only appear with a strain larger than 1.57. For the customized extensional rheometer, parameters including extensional temperature, rate, and time can be well controlled, and it can be easily coupled with *in situ* characterization techniques, i.e., IR and x-ray scattering.

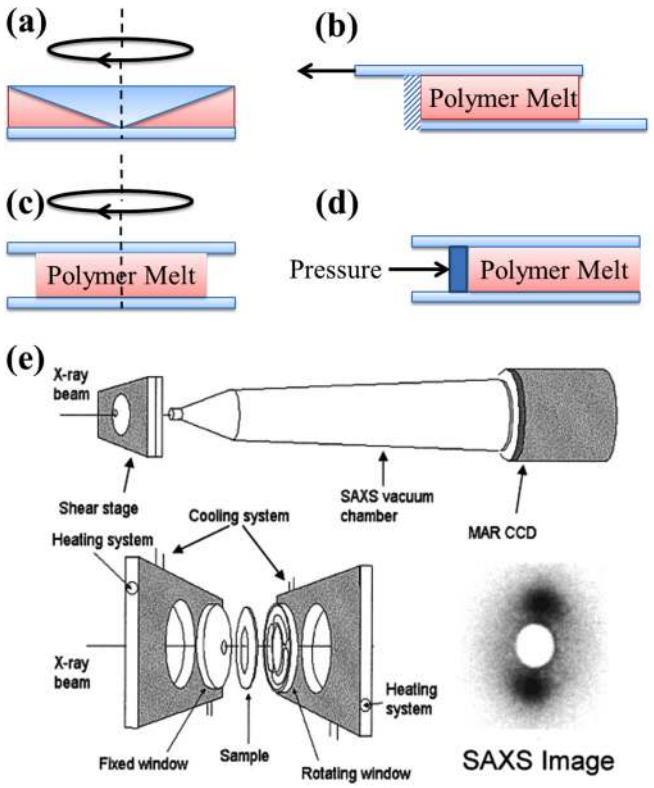

FIG. 9. Schematic illustration of different shear geometries: (a) cone-plate, (b) rectilinear parallel plates, (c) rotating parallel plates, and (d) slot flow. (e) The setup of the Linkam shear stage in synchrotron radiation x-ray scattering beamline. Reproduced with permission from Somani *et al.*, Macromolecules **33**(25), 9385–9394 (2000). Copyright 2000 American Chemical Society.

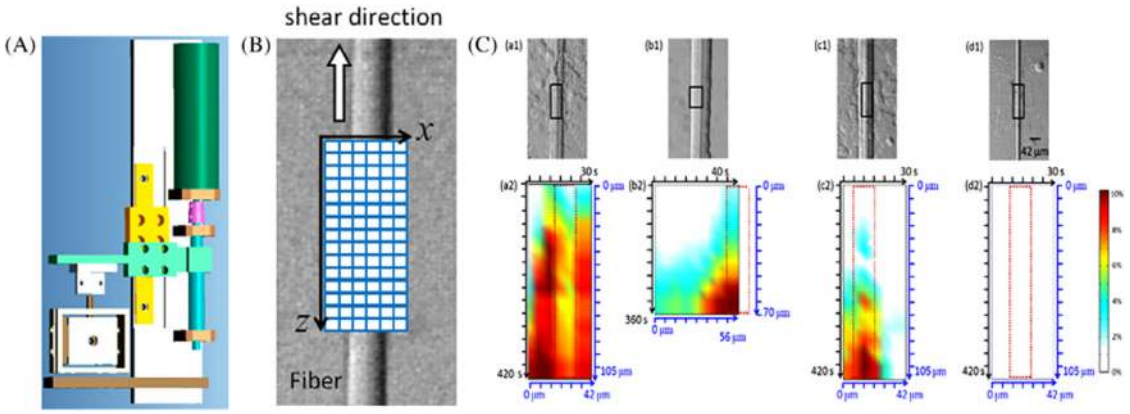

FIG. 10. (A) Schematic illustration of the setup of the shear apparatus for FIC, where the shear is achieved by the fiber. (B) Optical microscopy picture of real shearing and detection region for micro-focus SRXS. (C) Optical microscopy pictures of the *i*-PP sample after shearing at a temperature of (a) 160, (b) 170, (c) 175, and (d) 180 °C, together with a corresponding contour plot of crystallinity as captured by micro-focus SRXS. Reproduced with permission from Su *et al.*, Macromolecules **47**(13), 4408–4416 (2014). Copyright 2014 American Chemical Society.

2. Shear flow

Despite the extensional mode, another common method to apply external flow is shearing. There are numerous modes for shearing, i.e., cone-plate [Fig. 9(a)],[49] rectilinear parallel plates [Fig. 9(b)],[50,51] rotating parallel plates [Fig. 9(c)],[52,53] and slot flow [Fig. 9(d)].[44,54] Both cone-plate and rectilinear parallel plates provide a uniform shear rate, whereas the other two show the shear rate gradient. Here, one most widely used shear stage—the Linkam shear stage, or more specifically Linkam CSS450—is presented. The Linkam shear stage is based on the rotating parallel plates. Figure 9(e) shows a typical setup of the Linkam shear stage in the synchrotron radiation x-ray scattering beamline.[55] Such shear rate gradient leads to more convenient detection of FIC under different shear rates. Also, all measurements could be done with a fixed temperature, which eliminates possible uncertainty reproducing the thermal history with repeated measurements for different shear rates.

Despite above shear geometry, another kind of shear is achieved through the introduction of fiber. Figure 10(a) shows the design of a shearing device coupled with micro-focus SRXS, where fiber is used for applying the shear flow. The micro-focus x-ray scattering can provide a high spatial resolution of the whole sample after step shearing as shown in Fig. 10(b). Therefore, the detailed micro-structure evolution after step shearing can be obtained [Fig. 10(C)]. If the shearing is applied well above the melting temperature of the sample ($T_m = 165$ °C), no crystal is observed [Figs. 10(c)–2(d)]. Furthermore, cooling the temperature to 138 °C leads to the appearance of cylindrical crystallites together with enhanced crystallization kinetics. Also, as shown in Figs. 10(c)–10(c), an induction period is obtained when later crystallized at 138 °C. Such results suggest that the shear-induced precursor is non-crystalline, and sufficient time is required for transformation from non-crystalline state to crystalline one.[56]

3. Multidimensional flow

As discussed in Sec. II A, in the real industry, the multidimensional, rather than simple shear or extensional flow, would be encountered. Here, the biaxial stretching, portable extruder, and film blowing are selected typical examples to show recent efforts attempting to the *in situ* characterization of microstructural evolution under different flow conditions.

Figure 11(a) shows the design of a portable extruder which can be installed in the x-ray beamline of the synchrotron radiation facility.[57] The extruder is usually the first step for polymer processing. The flow field is not uniform as already shown in Fig. 2. The flow field condition can be controlled by the mandrel and extrusion piston. With the assistance of synchrotron x-ray scattering, Chang *et al.* investigated the influence of different extrusion conditions on the microstructure evolution of *i*-PP. Thus, obtained structural information together with the well-controlled rheological information provides sufficient hint for the correlation between flow parameters and microstructural evolution during extrusion.

Another frequently encountered flow is the biaxial stretching as shown in Fig. 11(b). Limited by the available space in the synchrotron beamline, the biaxial stretching machine needs to be minimized but kept the main feature of biaxial stretching. Chen *et al.* designed and successfully applied the biaxial stretching machine in BL16B of Shanghai Synchrotron Radiation Facility (SSRF), where the biaxial stretching of natural rubber was conducted.[58] With the continuous increase of the stretching ratio along with two perpendicular directions, it was found that the strain-induced crystallization (SIC) of natural rubber could be suppressed with $\lambda_x/\lambda_y < 1.6$. Such results challenge the widely accepted self-reinforcement mechanism of natural rubber under deformation.

The flow conditions become even more complicated during film blowing. As shown in Fig. 12, to mimic the film blowing process and meet the space requirement in synchrotron radiation beamline, the film blowing is minimized, whereas the key functions

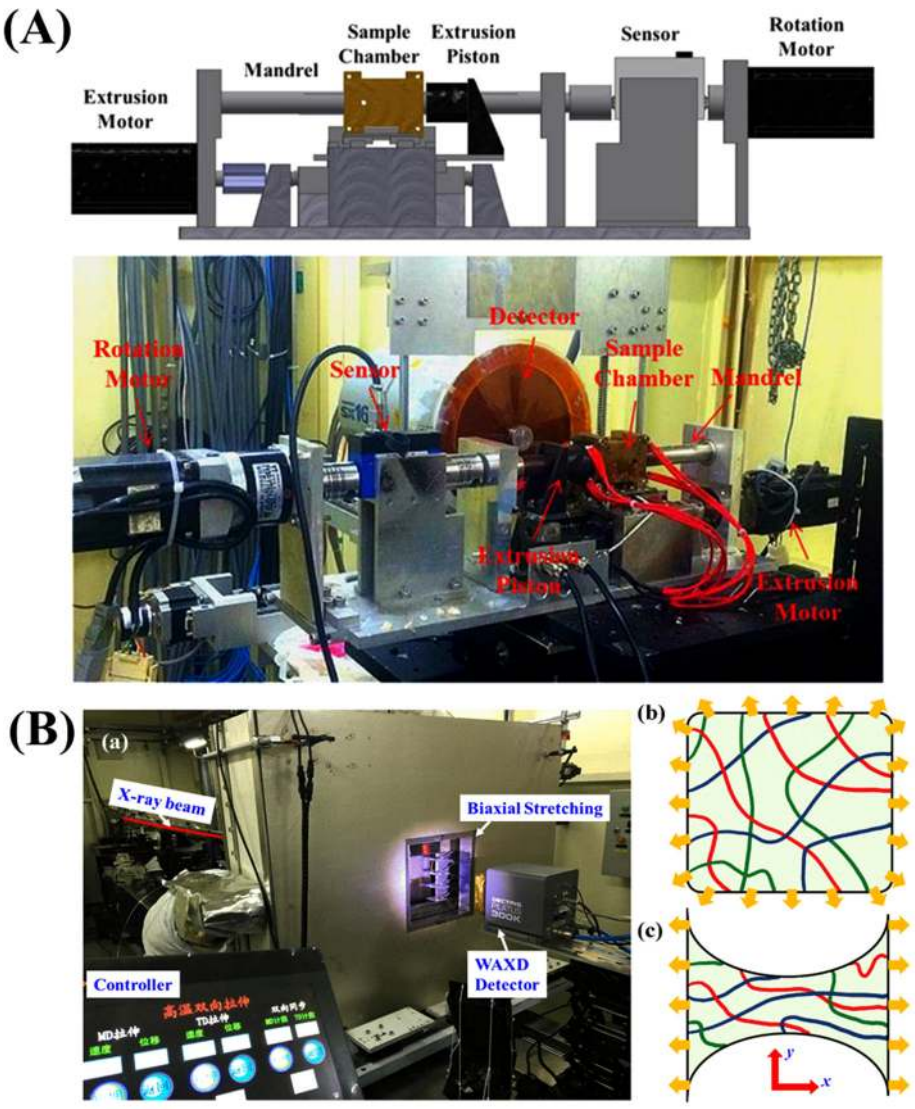

FIG. 11. (A) Schematic illustration of the portable extruder for *in situ* WAXS measurement together with the installed equipment in SSRF. Reproduced with permission from Chang *et al.*, Rev. Sci. Instrum. **89**(2), 025101 (2018). Copyright 2018 AIP Publishing LLC. (B) (a) The setup of the biaxial stretching machine in BL16B of SSRF; the comparison of (b) biaxial stretching and (c) uniaxial stretching. Reproduced with permission from Chen *et al.*, ACS Appl. Mater. Interfaces **11**(50), 47535–47544 (2019). Copyright 2019 American Chemical Society.

are the same as those of apparatus in the real industry.[59–65] The flow field during the film blowing process is intrinsically biaxial, where the horizontal extension of the bubble induced by blowing air and the vertical one induced by the nip rolls. Here, the flow is characterized by the particle tracking method where the particle is captured by CCD, and the temperature is detected by the infrared (IR) thermometer. The *in situ* synchrotron radiation x-ray scattering, WAXS/SAXS, was applied to capture the microstructure evolution right above the die. It was found that the crystallinity at the frost line, where the bubble diameter reaches the maximum, is determined by both external flow field and internal molecular characteristics of polymers. And the non-deformed crystal-based scaffold is formed at the frost line. Despite FIC, the temperature gradient exists during the film blowing process, namely, the temperature induced crystallization (TIC) competes with FIC through the whole process.[60]

The flow in real processing is always complicated. But the knowledge obtained by the above simple extension and shear rheometers is useful to understand the FIC in such non-uniform flow and temperature fields. Moreover, the final crystal morphology, either point-like or shish structure, can be obtained through proper selection of a polymer material and processing parameters.[60] The development of such *in situ* equipment provides great opportunities for researchers in both industry and academics to obtain the desired properties of polymer products.

B. Simulation

One great advantage of simulation is the capturing of the detailed molecular feature under flow. Utilizing non-equilibrium molecular dynamics (NEMD) simulations, the researchers can track

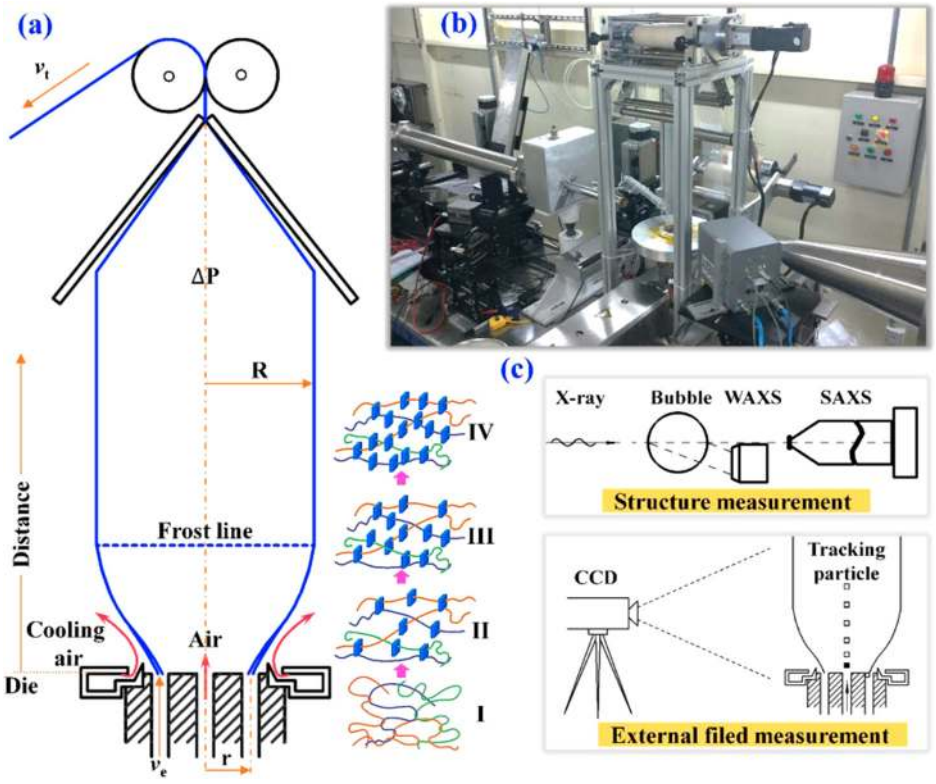

FIG. 12. (a) Schematic illustration of the film blowing process; (b) the customer-built film blowing machine installed in the synchrotron x-ray beamline 16B, Shanghai Synchrotron Radiation Facility (SSRF). (c) The *in situ* characterization methods, including WAXS/SAXS for microstructure and CCD for the flow field. Reproduced with permission from Zhao *et al.*, Polym. Test **85**, 106439 (2020). Copyright 2020 Elsevier.

the trajectory of every single monomer upon crystallization under flow, and the information at the molecular level is, therefore, accessible. The local/global order parameters are introduced in a simulation study to extract evolutions of many properties such as local structure, conformation, orientation, density, and crystallinity. In Fig. 13, the snapshots of systems clearly show the crystallization process of the polymer melt under extension flow, where the crystalline domains are colored in white.[66–68] Meanwhile, the structures within amorphous domains are identified, the distributions of folds (yellow), tie chains (red) and cilia (green) tell how the networks forming during FIC.

On the other hand, the thermodynamic quantities of polymer crystallization can be calculated by MD simulations even though the FIC is non-equilibrium in nature. Recently, Nicholson *et al.* developed a method based on the mean first passage time (MFPT) to quantitatively characterize the kinetics and physics of FIC.[69] In Fig. 14, how the critical free energy barrier (ΔG^*), the critical size of the nucleus (n^*), and the monomer attachment rate (f_1) change with shear rate (or Weissenberg number W_i) are given for both shear and extension flows. That information extracted from MD simulations shed some light on understanding polymer crystallization as the nucleation events at temporal and spatial resolutions that present particular challenges to the experiment.

IV. MOLECULAR ORIGIN OF FIC

In Secs. I–III, the general phenomena of FIC, i.e., crystal morphology and crystallization kinetics, and techniques used for tracking FIC are presented. In Sec. IV, the molecular origin of FIC will be addressed first, which could provide a theoretical explanation for the formation of different crystal morphologies.

A. Coil–stretch transition

Following Peterlin's work,[71] De Gennes theoretically predicted that an abrupt transition from a random coil to extended chain conformation, namely, coil–stretch transition (CST), when the strain rate $\dot{\varepsilon}$ exceeds a critical value ($\dot{\varepsilon}_c$) [Fig. 15(a)].[72] In CST, no stable intermediate chain conformation exists.[24] One parameter, namely, Deborah number $D_e = \dot{\varepsilon}^*\tau_c$, can be used to quantify such phenomenon: $\dot{\varepsilon}$ is the macroscopic strain rate, and τ_c is the terminal relaxation time of the polymer chain, which is closely related to the molecular weight.

Later on, Keller and Kolnaar first validated this prediction through the elegant design of the extensional flow device as shown in Fig. 15(b).[70] The birefringence of PE dilute solution starts to change abruptly when the CST happens [Fig. 15(c)]. The results also show that the critical strain rate $\dot{\varepsilon}_c$ is molecular weight dependence: $\dot{\varepsilon}_c \propto M^{-1.5}$. Therefore, the longer chain is more easy to be stretched. This provides a hint for the mechanism for the formation of the shish–kebab structure, where the long-chain mostly participates in the shish formation.

The direct visualization of the CST of the single polymer chain is also achieved in the fluorescently labeled DNA system.[73–78] The experimentally direct visualization of the CST is merely valid

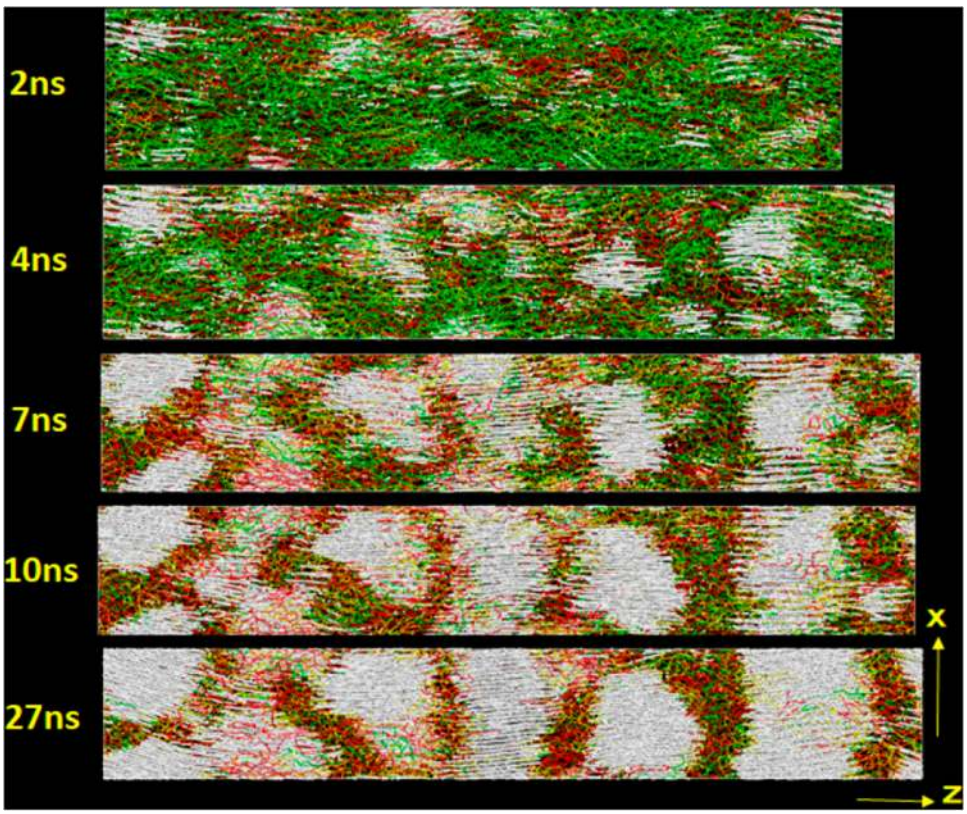

FIG. 13. The development of the network during crystallization, and the snapshots are extracted from the trajectory of MD simulations. Reproduced with permission from Yamamoto *et al.*, Macromolecules **52**(4), 1695–1706 (2019). Copyright 2019 American Chemical Society.

in the dilute solution of the macromolecules with long Kuhn lengths, such as DNA or protein. The direct visualizations of common commercial polymers are not accessing in the experiments. The molecular dynamics (MD) simulation provides a good supplement for the study of CST in the polymer systems.[77–82] The MD simulations extend the study of CST into the situation of stronger external fields and variable polymer systems including solutions of linear polymers, branched polymers, ring polymers, and tethered polymers.

Although CST originally proposed to describe the chain dynamics of the polymer chain under flow in dilute solution, the extension of CST to the concentrated solution and even the melt state is also attempted. Different from the polymer chain in the dilute solution, the polymer chains in the concentrated solution and melt are highly entangled with each other. In other words, the polymer network, rather than a single chain, starts to be considered in dealing with the mechanism for the formation of flow-induced morphology.[70] As shown in Fig. 16 by Keller, further increasing the strain rate to $\dot{\varepsilon}_n$ leads the whole polymer chains deform as a network. The two lines of $\dot{\varepsilon}_c$ and $\dot{\varepsilon}_n$ get close to each other with increasing the concentration. If there is no crossover between these two lines, the CST holds for both the solution and the melt state as shown in Fig. 16(a). Otherwise, CST holds for concentration below C^*, and for the melt state, the molecular origin needs to be revised. However, the prerequisite for the foundation of CST is the hydrodynamic effect, which exists in a dilute solution case. In other words, for the homopolymer, the theoretical foundation of CST in the melt or highly entangled states does not exist anymore.[12] The sudden transition from a random coil state to a stretched one would be replaced by transient transition with multiple intermediate states.

B. Stretched network model

In addition to CST, there exist other models accounting for the formation of shish–kebab structure formation. Among them, the stretched network model stands out due to its success in explaining the formation of the shish–kebab structure in a highly entangled state. As early as 1984, Smook and Pennings proposed that the stretched network during flow is responsible for the formation of the shish–kebab structure during gel spinning as shown in Fig. 17.[83,84] For the ultra-high molecular weight PE (UHMWPE), highly entangled network is formed in the gel state before spinning, and the elastic flow instability is also encountered at a low flow rate. During extrusion, the inhomogeneous network consisting of entanglements of different lifetime deforms inhomogeneously: the entanglement with short lifetime migrates or relaxes easily, while that with long lifetime bears the external flow leading to the formation of oriented chains. During the continuous flow, the oriented chains form the shish while the unoriented ones form the kebab.

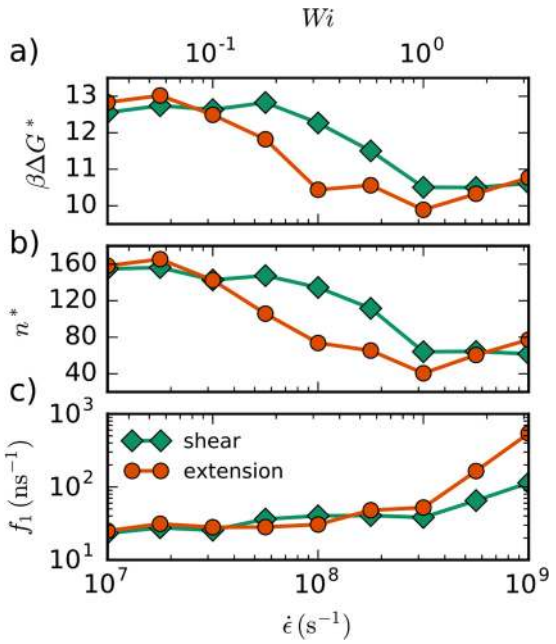

FIG. 14. The change of (a) critical free energy barrier, (b) critical size of nucleus, and (c) monomer attachment rate when increasing shear and flow rate. Reproduced with permission from Nicholson *et al.*, J. Chem. Phys. **145**(24), 244903 (2016). Copyright 2016 AIP Publishing LLC.

For the polymer melt under flow, Janeschitz-Kriegl *et al.* introduced the dormant nuclei, which is intrinsically a precursor with a shape of fringed micelle.[86–88] Once the flow strength exceeds the critical value, those dormant nuclei would transform into point-like nuclei and align along the flow direction. And further increasing the flow strength leads to the merge of these nuclei to form the shish-like nuclei. Later on, some modified models are also proposed. Figure 18 shows one model proposed by Seki *et al.* for depicting the molecular picture of the formation of nucleation by

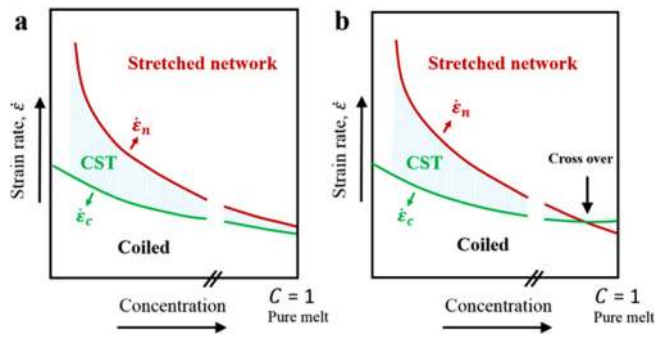

FIG. 16. The critical strains for CST ($\dot{\epsilon}_c$) and network formation ($\dot{\epsilon}_n$) in strain rate and concentration space (a) without and (b) with crossover. Reproduced with permission from Keller and Kolnaar, Prog. Colloid Polym. Sci. **92**, 81–102 (1993). Copyright 1993 Springer Nature.

the flow.[85] The flow could lead to the formation of precursors close to the initial nucleus, and these precursors would be further transformed into more thermal stable nucleus along the flow field. This eventually leads to the trace of precursor clusters or, namely, shish nuclei. Later, Cui *et al.* proposed a ghost nucleation model, which highlights the importance of the movement of these precursors for the formation of shish nuclei and enhanced crystallization kinetics.[89] Despite existing different models, the key feature induced by the flow is the significant reduction of the nucleation barrier. As a result, a more point-like nucleus or shish-nucleus could be formed under flow.

In all, for the highly entangled polymer, concentrated polymer solution, or melt states, the entanglement between physically cross-linking points, rather than the single-chain, is responsible for the shish–kebab structure formation.

C. Multi-step ordering of flow-induced nucleation

With the fast development of characterization techniques as mentioned above, a more detailed transient structure, especially the

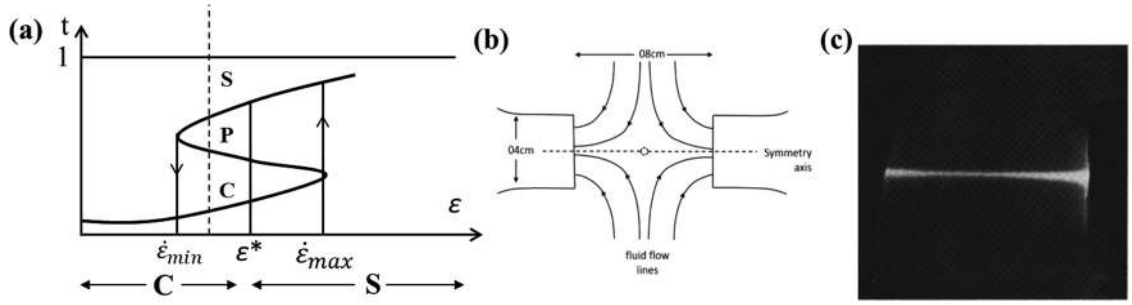

FIG. 15. (a) Illustration of the coil–stretch transition of a polymer chain in dilute solution as predicted by De Gennes.[72] Transition happens within ($\dot{\varepsilon}_{min} - \dot{\varepsilon}_{max}$), where $\dot{\varepsilon}_{min}$ and $\dot{\varepsilon}_{max}$ are the orders of inversion of the Rouse and Zimm frequency, respectively. And within this range, three possible states exist: a coiled state *C*, an unstable state *P*, and the stretched state *S*. The CST happen at $\epsilon = \epsilon^*$. Reproduced with permission from De Gennes, J. Chem. Phys. **60**(12), 5030–5042 (1974). Copyright 1974 AIP Publishing LLC. (b) Schematic illustration of the device used by Keller with two opposite jets. (c) The birefringent line observed for PE dilute solution under flow. Reproduced with permission from Keller and Kolnaar, Prog. Colloid Polym. Sci. **92**, 81–102 (1993). Copyright 1993 Springer Nature.

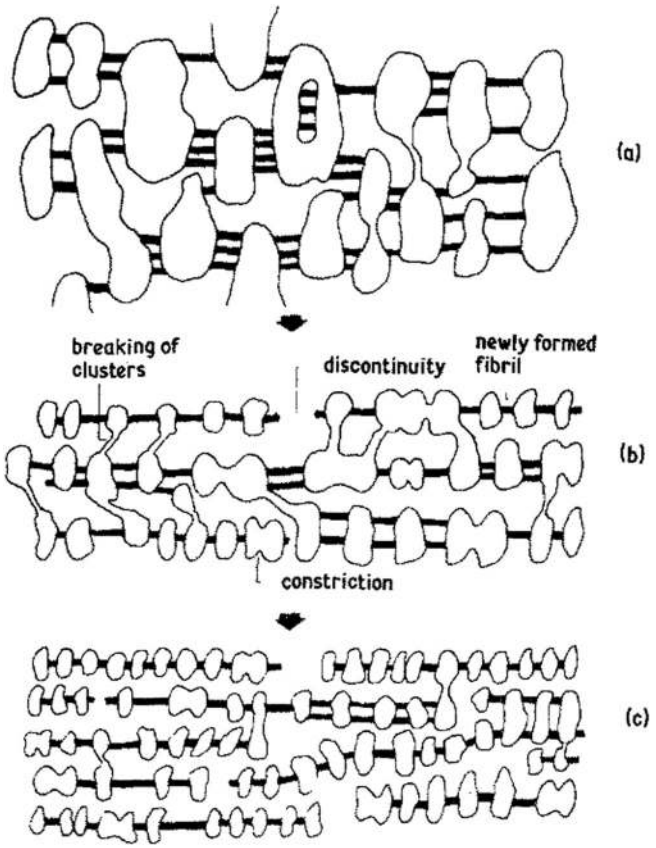

FIG. 17. Illustration of the flow scheme of UHMWPE during gel spinning, where the bundles of the oriented molecule (dark line) and a cluster of unoriented molecules form alternatively. Adapted with permission from Smook and Pennings, J. Mater. Sci. **19**(1), 31–43 (1984). Copyright 1984 Springer Nature.

initial flow induce nucleation (FIN), can be obtained. The initial microstructural evolution, or the FIC precursor structure, has been extensively investigated by numerous research groups, i.e., Li and de Jeu,[42,90] Hsiao *et al.*,[33,91–94] Winter *et al.*,[95–98] Kornfield *et al.*,[44,85,99–101] Peters *et al.*,[25–28] and our group[46,56,102–105] (just a few are listed here limited by the length of the current article). Numerous discoveries are found. For instance, the structure of shish can be either amorphous or crystalline, and not all chains within shish are fully extended but share the same molecular feature: chains in shish are highly oriented along the flow direction.[24] Here, the multi-step ordering of FIN is presented as a general view of the current understanding of the formation of nucleation under flow.

As shown in Fig. 19, after applying the flow on the polymer melt, the random coil immediately experiences transition from the random coil to the helix.[106] Later, these rigid helixes start the isotropic–nematic transition to form a locally anisotropic structure.[107,108] Then, the helix bundles are formed as the precursors for nucleation and growth. Concerning the direct experimental evidence of the existence of these intermediate states, the IR[43] or Raman[109] spectroscopy is extensively used to track the formation of the helix as these techniques are sensitive to local chain conformation change. For *i*-PP case, different helix lengths result in different and well-resolved IR absorption lines.[110–112] Numerous rheo-IR experiments were conducted to *in situ* observe the coil–helix transition.[43,113,114] The non-equilibrium MD simulation is also used to investigate the conformational transition of *i*-PP under extension,[115] where more detailed microstructure information including the number and the length of the helix can be quantitatively calculated from the trajectories. These spectroscopy and simulation results together confirm the multi-step ordering of FIN.

The multi-step feature of FIN is completely different from the "one-step" nucleation scenario described by classical nucleation theory (CNT)[116] but similar to "two-step" or "multi-step" nucleation as recently proposed in crystallization under quiescent conditions.[117–119] It has been observed that the Weissenberg number (W_i) and temperature together determine the kinetics of FIN.[118,120] The slow strain rate ($W_i < 1$) may not lead to a conformational change like the "*coil–helix*" transition of *i*-PP[89,113,121,122] and "*gauche–trans*" transition of PE,[123,124] thus the nucleation remains the same as that at the quiescent condition. When $W_i > 1$, the molecular chains will align and straighten along the direction of the flow field, which remarkably accelerate the nucleation kinetics, and the orientational ordering of segments occurs before the onset of crystallization.[118,125] Our group has studied the influence of temperature on the crystallization of polyethylene under flow,[120] when the shear applied at a temperature lower than the equilibrium melting temperature (T_m^0), the crystallization kinetics is enhanced and follows the same pathway as quiescent condition, which is local ordered structure fluctuation assisted nucleation. Nevertheless, when the system is sheared at a temperature higher than T_m^0, the density fluctuation takes place before crystallization, and the crystallization kinetics becomes conformational ordering → density fluctuation → nucleation. In Fig. 20, the snapshots present the spatial distributions of density (Voronoi Volume), oriented ordered segments (*CO* parameter), and the clusters in the system. The CO parameter is calculated by

$$\mathrm{CO} = l^2 \times (2P(\theta) + 1), \tag{1}$$

where $P(\theta) = (3\cos^2\theta - 1)/2$ is the orientation parameter and l is the length of all-*trans* segments. Higher CO value indicates that the conformational ordered segments have a longer length and higher orientation. The regions with a higher CO value correspond to high-density domains in the system, and within these high-density domains, the nucleation takes place subsequently. This picture suggests that the FIN may be a multi-step ordering process with density fluctuation as the intermediate state.

Many research groups have made a great contribution to this issue using computational techniques, i.e., Muthukumar *et.al.*,[126–128] Rutledge *et al.*,[129,130] Sommer *et al.*,[131–133] Hu *et al.*,[134–136] and Yamamoto[137–139] (just a few are listed here due to the length limitation). The microscopic evidence can be a compensation of experimental results and also shed some light on the fundamental understanding of this non-equilibrium crystallization process.

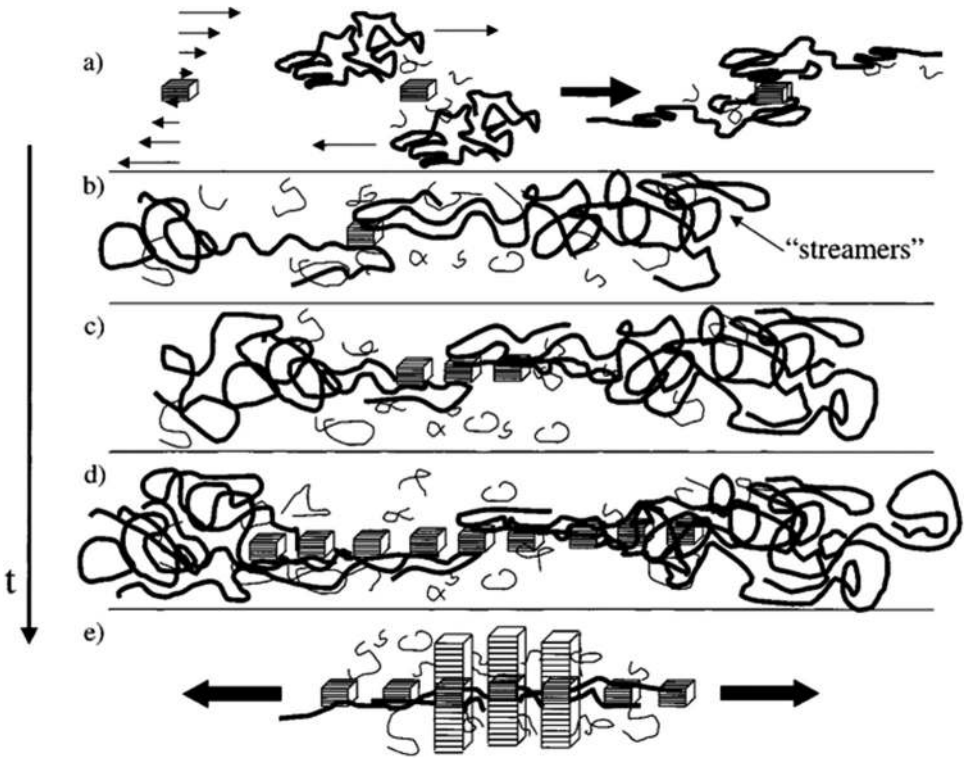

FIG. 18. Schematic illustration of the nature of the shear-induced nucleation together with subsequent lateral growth of oriented lamellae above the threshold shear stress.[85] (a) The long-chain (bold line) adsorbs onto the point-like nucleus, whereas the dangling segment becomes oriented during external shear. (b) More chains adsorb this nucleus and their dangling segment forms "streamers" close to the existing nuclei. (c) More nuclei appear due to the increased local segment orientation. (d) More chains adsorb to these formed nuclei and align along the shearing direction. (e) The lateral growth perpendicular to the shearing direction. Reproduced with permission from Seki *et al.*, Macromolecules **35**(7), 2583–2594 (2002). Copyright 2002 American Chemical Society.

V. THERMODYNAMICS DESCRIPTION OF FIC

The molecular origin of FIC as discussed above mainly accounts for different crystal morphologies induced by flow, whereas the theoretical treatment of the enhanced crystallization kinetics during FIC is still missing. Herein, the thermodynamics description of FIC will be presented. Although the FIC is an intrinsically non-equilibrium state, the FIC can still be treated by classical thermodynamics concepts, especially for that in weak flow conditions.

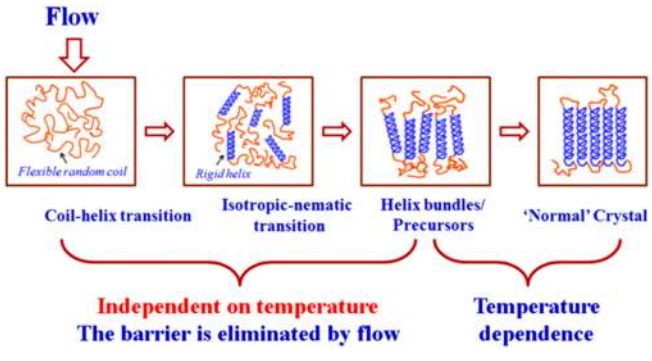

FIG. 19. Molecular description of the microstructure evolution of FIC from the initial random coil in the melt state to the final crystalline state. The multiple intermediate states exist, including coil–helix transition, isotropic–nematic transition, and the formation of nucleus through the packing of bundles. Reproduced with permission from Wang *et al.*, Macromolecules **49**(5), 1505–1517 (2016). Copyright 2016 American Chemical Society.

A. Entropy reduction model (ERM)

The first experimental evidence of FIC is believed to be attributed to Penning's work in the 1960s, where the later well-known *shish–kebab* structure is found.[19,20] However, almost two decades ago, Flory proposed a model, namely, entropy reduction model (ERM), accounting for the strain-induced crystallization (SIC) in natural rubber.[140] The ERM is extensively used in understanding FIC and owns great success in interpreting the enhanced nucleation rate.

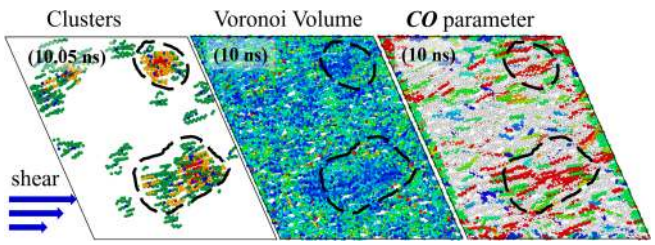

FIG. 20. The snapshot of the non-equilibrium MD simulation of polyethylene. The well overlapped spatial distribution of high CO region, high-density domain, and nuclei suggests that crystallization takes place via density fluctuation under flow. Reproduced with permission from Tang *et al.*, J. Chem. Phys. **149**(22), 224901 (2018). Copyright 2018 AIP Publishing LLC.

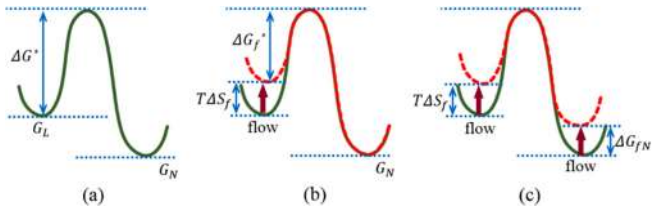

FIG. 21. Schematic illustration of the thermodynamics description of the flow-induced nucleation. (a) Classical nucleation barrier for crystallization under quiescent condition; (b) the reduced nucleation barrier induced by the external flow, but the Gibbs free energy of the nuclei remains unchanged; and (c) both the Gibbs free energy of the initial melt and final nuclei are reduced under flow leading to apparent reduction of the nucleation barrier. Reproduced with permission from Wang *et al.*, Macromolecules **49**(5), 1505–1517 (2016). Copyright 2016 American Chemical Society.

The classical nucleation theory describes the nucleation rate as[116,141]

$$I \cong \frac{Nk_BT}{h}\exp\left(-\frac{\Delta G^* + \Delta G_\eta}{k_BT}\right), \tag{2}$$

where h and k_B are Plank and Boltzmann constants, respectively; N is the total number of particles in the system; and T is the temperature (K). ΔG^* represents the maximum activation free energy for nucleus formation as shown in Fig. 21(a), and ΔG_η represents the free energy for one particle diffusing from the melt to crystalline domains.

For polymer, due to the connectivity of the segment, the initial melt is no longer isotropic under flow. As a result, the polymer chain in the deformed melt already deviates from the initial random coil state or the Gaussian chain. This is the origin of the name "strain-induced crystallization," where strain here represents the deviation of the polymer chain from the initial Gaussian state. As shown in Fig. 21(b), such deviation results in the increase in the free energy of the polymer chain in the melt state and finally reduces the nucleation barrier ΔG_f^* for the formation of the nucleus. One great success of ERM is the estimation of the reduction of ΔG^* in Eq. (2). Rooted in the rubber elasticity theory, the free energy reduction of the oriented polymer melt is attributed to conformation entropy reduction ΔS_f, which can be estimated by the statistical mechanics. Based on ERM, $\Delta S_f = \left(\frac{k_B\bar{N}}{2}\right)\left[\left(\frac{24\,m}{\pi}\right)^{0.5}\lambda - \left(\lambda^2 + \frac{2}{\lambda}\right)\right]$, where λ is the stretch ratio, and m and $\bar{N}$ are the numbers of Kuhn segment per network chain and network chain per unit volume, respectively.[140,142] Therefore, the reduced ΔG_f^* can be quantitatively calculated.

B. Modified ERM

In ERM, the simple affine deformation works quite well for the natural rubber system as the system is highly crosslinked. Concerning the polymer melt, however, only physical entanglements exist in most real applications. Therefore, the chain dynamics is required to be considered. Later on, based on the Doi–Edwards model and independent alignment approximation,[13,143] a microrheological model, namely, (DE-IAA), was proposed.[144] The key feature of this model is the modification of the free energy of the polymer melt under steady flow. The free energy is calculated based on the strain rate and chain relaxation (DE memory function), which is, thus, strain rate dependent. Besides the chain relaxation under steady flow, such relaxation occurs also after the flow. Tian *et al.* designed a step-strain experiment to check the influence of the strain rate on the nucleation rate.[145] A significant reduction of the entropy change is found after the flow, which is attributed to chain relaxation. In all, despite numerous modifications of calculation of the free energy of the polymer melt under flow, the general scenario as shown in Fig. 21(b) does not change.

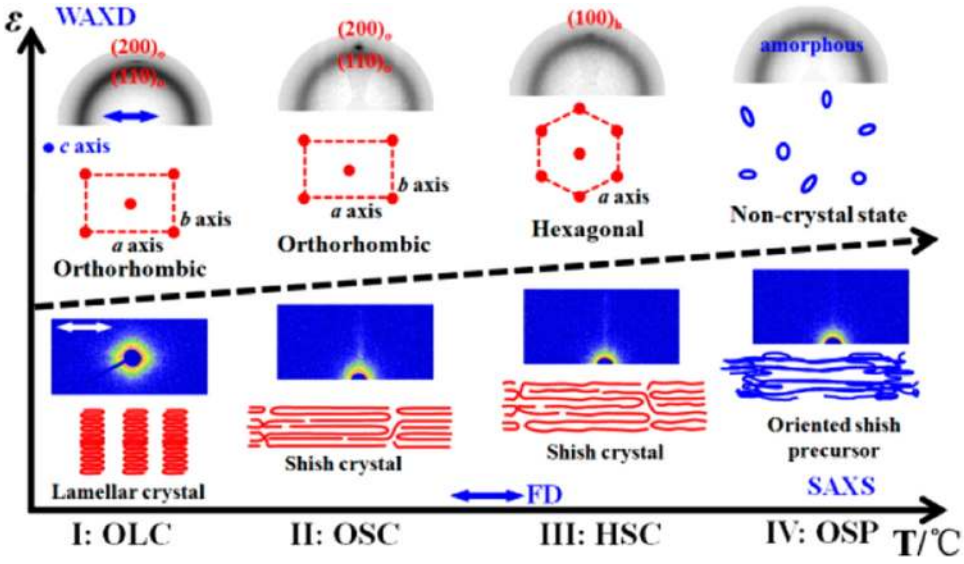

FIG. 22. Schematic illustration of different crystal morphologies in strain–temperature space after extensional flow. Reproduced with permission from Liu *et al.*, Macromolecules **47**(19), 6813–6823 (2014). Copyright 2014 American Chemical Society.

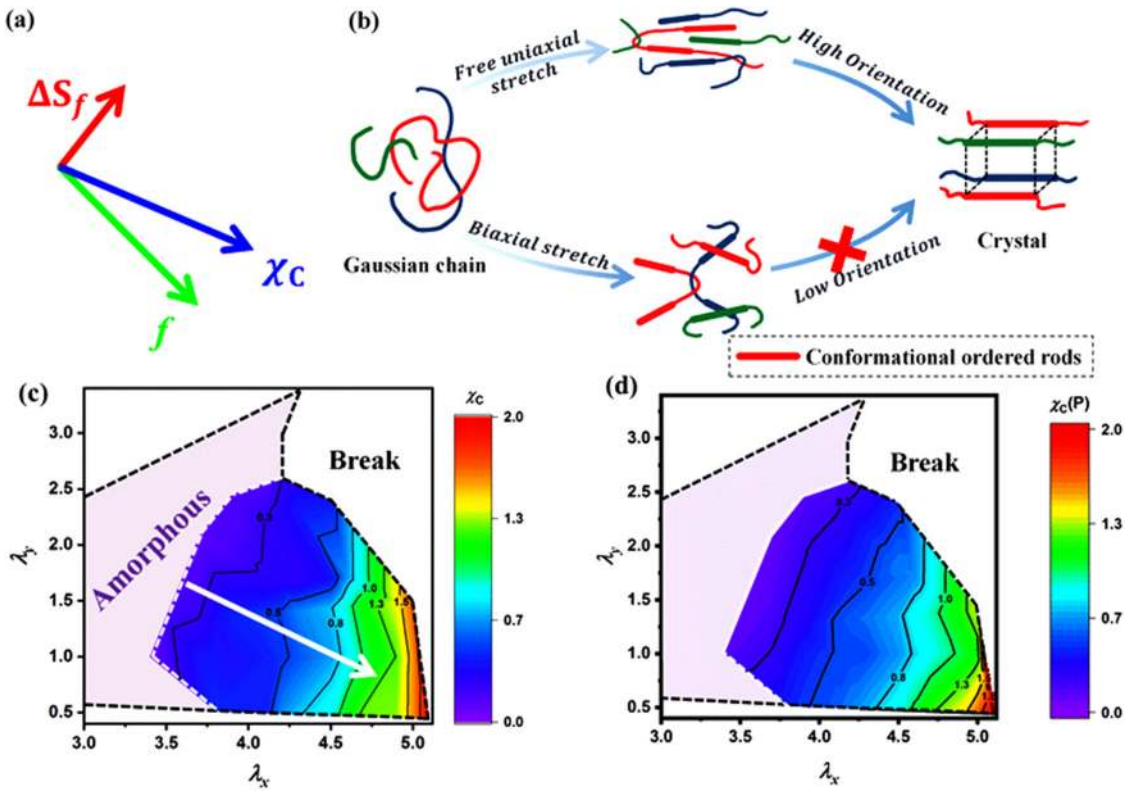

FIG. 23. (a) Illustration of the contributions of entropy ΔS_f and segmental orientation f to the overall crystallinity χ_c. (b) The comparison of the uniaxial and biaxial stretching; (c) the experimentally obtained crystallinity in λ_x vs λ_y space, together with the (d) theoretical fitted one. Reproduced with permission from Chen *et al.*, ACS Appl. Mater. Interfaces **11**(50), 47535–47544 (2019). Copyright 2019 American Chemical Society.

Despite the free energy change of the initial polymer melt induced by flow, that of the formed crystal may also be changed. Liu *et al.* found four different crystal morphologies of lightly cross-linked PE after flow, namely, orthorhombic lamellar crystal (OLC), orthorhombic shish crystal (OSC), hexagonal shish crystal (HSC), and non-crystalline oriented shish precursor (OSP) (Fig. 22).[103] This finding shows that the invariant crystal structure assumed in classical ERM is not right anymore. The local packing structure (crystal phase) and crystal morphology changes, i.e., from point-like to shish, clearly showing the final free energy should be changed as shown in Fig. 21(c).

Based on the entropy reduction of the initial melt and free energy change of the final nucleus, a unified entropy reduction–energy change (ER–EC) model is proposed. Based on the ER–EC model, two key parameters, namely, stretch ratio λ and homogeneous crystallization temperature can be expressed as[103]

$$\frac{1}{T_c(\lambda)} = \frac{1}{T_C(1)} - \frac{\nu k_B\left(\lambda^2 + \frac{2}{\lambda} - 3\right)}{2\Delta H\left(1 - \frac{4\sigma_e}{\Delta H l^*}\right)}, \tag{3}$$

where $T_C(1)$ and $T_c(\lambda)$ represent the crystallization temperatures at elongation ratios of 1 and λ, respectively; ν is the network-chain density; l^* represents the critical nucleus thickness; and σ_e and ΔH are the surface energy and the enthalpy change of the newly formed nucleus, respectively. Equation (3) considers not only the entropy reduction of the initial melt under flow but also the specific crystal packing structure (ΔH) and shape (l^* and σ_e) of the newly formed nucleus.

In summary, to interpret the enhanced nucleation rate induced by flow, various models, including ERM, DE-IAA, and ER–EC, are proposed based on the classical nucleation theory. However, this classical theory has been challenged during the last two decades, especially in the crystallization of small molecules.[146] Various new proposed models, i.e., crystallization by particle attachment (CPA),[146] are proposed, which mostly thanks to the fast development of new characterization techniques (i.e., Cryo-TEM). Systems, such as inorganic salt[147–149] and bio-systems,[150,151] have shown the multi-step crystallization mechanism. Concerning the polymer system, such a multi-step feature has also been discovered. Readers are referred to a recent review.[12]

Either ERM or modified version mostly accounts for the FIC under uniaxial deformation. However, in real service conditions,

the multidimensional flow field is more frequently encountered, i.e., film blowing and biaxial processing of the polymer film. Despite numerous investigation of FIC under uniaxial deformation, those under biaxial stretching are quite few. One great challenge comes from the suitable equipment, i.e., the biaxial stretching machine that can be installed in the synchrotron radiation beamline. Chen *et al.* recently reported detailed microstructure evolution of nature rubber under biaxial stretching with the assistance of the custom-built biaxial stretching machine.[58] Different from uniaxial stretching, the contribution of the conformation entropy reduction ΔS_f and segmental orientation f to the nucleation barrier can be obtained as illustrated in Fig. 23(a). The nucleation barrier [Eq. (2)] expressed in ERM only considers the contribution of the conformational entropy reduction, whereas the segmental orientation f is missing. Considering the contribution of the segmental orientation f [Fig. 23(b)], the nucleation barrier can be expressed as

$$\begin{aligned}\Delta G_f^* &= \Delta G_f^* - T\Delta S_f - (T\Delta S_{ori} + \Delta U_{ori}),\\ &= \Delta G_f^* - T\Delta S_f - (af^2 + bf^3 + cf^4),\end{aligned} \tag{4}$$

where $(T\Delta S_{ori} + \Delta U_{ori})$ represents the contribution of the oriented segment, which can be further expressed as a Maier–Saupe relation of Hermans' orientation factor f. Based on Eq. (4), the calculated crystallinity χ_c as shown in Fig. 23(d) is well consistent with the experimental obtained one [Fig. 23(c)]. The proposed model in this work provides a new pathway in dealing with the FIC under the multidimensional flow field.

VI. CONCLUSIONS

In this tutorial, the general description of the flow-induced crystallization (FIC) was achieved generally through two lines: one is the detailed molecular picture for the formation of different crystal morphologies induced by flow, and the other is the general thermodynamics consideration for enhanced crystallization kinetics induced by the flow. The important models and theories, including the coil–stretch transition theory, the stretched network model, and the entropy reduction model are briefly discussed. Herein, the basic foundations of FIC together with recent achievements are summarized.

Considering the publication of Flory's work in 1947,[140] people have continued working on FIC for more than 70 years. Yet, there are still numerous debates existing. This reflects the huge difficulty in fully understanding FIC. Since the FIC is closely related to industrial application, the continuous effort in understanding FIC and implementing new characterizations to *in situ* track the microstructure evolution of FIC is required. Since quite few structure features exist in the early stage of FIC, namely, the direct detection of multiple intermediates, different techniques validating various intermediate structures of different polymers are required. The fast development of molecular dynamics simulation and advanced characterization techniques, i.e., synchrotron radiation facility, presents a greatly promising future to investigate this non-equilibrium FIC. For instance, the x-ray photon correlation spectroscopy (XPCS) has been successfully coupled with 3D printing technology to *in situ* track both structure and dynamics evolution during injecting.[152] The further deep investigation of the "old" FIC will continuously help us to better understand different crystal morphology formations during various processing, and optimization of both external processing parameters, i.e., strain rate and time, and internal molecular characteristics of polymers, i.e., molecular weight and polydispersity.

ACKNOWLEDGMENTS

We appreciate the funding support from the National Natural Science Foundation of China (NNSFC; Nos. 51633009 and 51703217), the National Key R&D Program of China (No. 2016YFB0302500), and the Fundamental Research Funds for the Central Universities (No. WK2310000079). We would like to acknowledge the kind help of co-workers in the National Synchrotron Radiation Laboratory (NSRL) and Shanghai Synchrotron Radiation Facility (SSRF) for beamtime and assistance in conducting experiments during last 15 years. Also, we would like to thank Professor Zhe Ma, Professor Tian Nan, Dr. Kunpeng Cui, and Professor Zhen Wang for their helpful comments on the manuscript.

NOMENCLATURE

CNT	Classical nucleation theory
CO	Conformational order
CPA	Crystallization by particle attachment
CST	Coil–stretch transition
De	Deborah number
DE-IAA	Doi–Edwards-independent alignment approximation
ERM	Entropy reduction model
FIC	Flow-induced crystallization
FIN	Flow-induced nucleation
MD	Molecular dynamics
NEMD	Non-equilibrium molecular dynamics
PE	Polyethylene
PP	Polypropylene
SAXS/WAXS	Small/Wide angle x-ray scattering
SIC	Strain-induced crystallization
SRXS	Synchrotron radiation x-ray scattering
TIC	Temperature induced crystallization
Wi	Weissenberg number
XPCS	X-ray photon correlation spectroscopy

DATA AVAILABILITY

Data sharing is not applicable to this article as no new data were created or analyzed in this study.

REFERENCES

[1]R. Geyer, J. R. Jambeck, and K. L. Law, "Production, use, and fate of all plastics ever made," Sci. Adv. **3**(7), e1700782 (2017).
[2]S. Z. D. Cheng, *Phase Transitions in Polymers: The Role of Metastable States* (Elsevier, 2008).
[3]J. D. Hoffman and R. L. Miller, "Kinetics of crystallization from the melt and chain folding in polyethylene fractions revisited: Theory and experiment," Polymer **38**, 3151–3212 (1997).

[4]J. D. Hoffman and J. I. Lauritzen, "Crystallization of bulk polymers with chain folding: Theory of growth of lamellar spherulites," J. Res. Natl. Bur. Stand. A Phys. Chem. **65A**(4), 297 (1961).
[5]M. Zhang, B.-H. Guo, and J. Xu, "A review on polymer crystallization theories," Crystals **7**(1), 4 (2017).
[6]K. A. Armitstead, Y. Chujo, P. Corradini, M. Fischer, G. Goldbeck Wood, G. Guerra, A. Halperin, H.-H. Kausch, A. Keller, J. E. Kennedy, B. Keszler, T. P. Lodge, T. Q. Nguyen, T. Saegusa, M. Stature, and M. Tirrell, "Polymer crystallization theories," in *Macromolecules: Synthesis, Order and Advanced Properties* (Springer, Berlin, 1992), pp. 219–312.
[7]B. Lotz, T. Miyoshi, and S. Z. D. Cheng, "50th anniversary perspective: Polymer crystals and crystallization: Personal journeys in a challenging research field," Macromolecules **50**(16), 5995–6025 (2017).
[8]G. Strobl, "Crystallization and melting of bulk polymers: New observations, conclusions and a thermodynamic scheme," Prog. Polym. Sci. **31**(4), 398–442 (2006).
[9]G. Strobl, "Colloquium: Laws controlling crystallization and melting in bulk polymers," Rev. Mod. Phys. **81**, 1287–1300 (2009).
[10]X. Tang, W. Chen, and L. Li, "The tough journey of polymer crystallization: Battling with chain flexibility and connectivity," Macromolecules **52**, 3575–3591 (2019).
[11]G. W. M. Peters, L. Balzano, and R. J. A. Steenbakkers, "Flow-induced crystallization," in *Handbook of Polymer Crystallization* (Wiley, 2013), pp. 399–432.
[12]K. Cui, Z. Ma, N. Tian, F. Su, D. Liu, and L. Li, "Multiscale and multistep ordering of flow-induced nucleation of polymers," Chem. Rev. **118**, 1840–1886 (2018).
[13]M. Doi and S. F. Edwards, *The Theory of Polymer Dynamics* (Oxford University Press, 1988).
[14]J. A. Kornfield, G. Kumaraswamy, and A. M. Issaian, "Recent advances in understanding flow effects on polymer crystallization," Ind. Eng. Chem. Res. **41**(25), 6383–6392 (2002).
[15]M. M. Denn, *Polymer Melt Processing* (Cambridge University Press, Cambridge, 2008).
[16]A. Keller and H. W. Kolnaar, "Flow-induced orientation and structure formation," In *Processing of Polymers*, edited by H. E. Meijer (VCH, New York, 1997), Vol. 18, pp. 189–268.
[17]A. J. Lovinger, "Twisted crystals and the origin of banding in spherulites of semicrystalline polymers," Macromolecules **53**(3), 741–745 (2020).
[18]P. J. Barham and A. Keller, "High-strength polyethylene fibres from solution and gel spinning," J. Mater. Sci. **20**, 2281–2302 (1985).
[19]A. J. Pennings and A. M. Kiel, "Fractionation of polymers by crystallization from solution, III. On the morphology of fibrillar polyethylene crystals grown in solution," Kolloid-Zeitschrift Zeitschrift für Polym. **205**(2), 160–162 (1965).
[20]A. J. Pennings, J. M. A. A. van der Mark, and H. C. Booij, "Hydrodynamically induced crystallization of polymers from solution II. The effect of secondary flow," Kolloid-Zeitschrift Zeitschrift für Polym. **236**(2), 99–111 (1970).
[21]J. Hoffman, "On the formation of polymer fibrils by flow-induced crystallization," Polymer **20**, 1071–1077 (1979).
[22]I. Lieberwirth, J. Loos, J. Petermann, and A. Keller, "Observation of Shish crystal growth into nondeformed melts," J. Polym. Sci. Part B Polym. Phys. **38**(9), 1183–1187 (2000).
[23]J. Petermann, M. Miles, and H. Gleiter, "The crystalline core of the row structures in isotactic polystyrene. I. nucleation and growth," J. Polym. Sci. Polym. Phys. Ed. **17**(1), 55–62 (1979).
[24]R. H. Somani, L. Yang, L. Zhu, and B. S. Hsiao, "Flow-induced Shish-Kebab precursor structures in entangled polymer melts," Polymer **46**(20), 8587–8623 (2005).
[25]J.-W. Housmans, G. W. M. Peters, and H. E. H. Meijer, "Flow-induced crystallization of propylene/ethylene random copolymers," J. Therm. Anal. Calorim. **98**(3), 693–705 (2009).
[26]G. W. M. Peters, F. H. M. Swartjes, and H. E. H. Meijer, "A recoverable strain-based model for flow-induced crystallization," Macromol. Symp. **185**(1), 277–292 (2002).
[27]H. Zuidema, G. W. M. Peters, and H. E. H. Meijer, "Development and validation of a recoverable strain-based model for flow-induced crystallization of polymers," Macromol. Theory Simul. **10**(5), 447–460 (2001).
[28]J. van Meerveld, G. W. M. Peters, and M. Hütter, "Towards a rheological classification of flow induced crystallization experiments of polymer melts," Rheol. Acta **44**(2), 119–134 (2004).
[29]E. Koscher and R. Fulchiron, "Influence of shear on polypropylene crystallization: Morphology development and kinetics," Polymer **43**(25), 6931–6942 (2002).
[30]I. Coccorullo, R. Pantani, and G. Titomanlio, "Spherulitic nucleation and growth rates in an IPP under continuous shear flow," Macromolecules **41**(23), 9214–9223 (2008).
[31]P. C. Roozemond, M. Van Drongelen, Z. Ma, A. B. Spoelstra, D. Hermida-Merino, and G. W. M. Peters, "Self-regulation in flow-induced structure formation of polypropylene," Macromol. Rapid Commun. **36**(4), 385–390 (2015).
[32]S. Coppola, L. Balzano, E. Gioffredi, P. L. Maffettone, and N. Grizzuti, "Effects of the degree of undercooling on flow induced crystallization in polymer melts," Polymer **45**(10), 3249–3256 (2004).
[33]B. S. Hsiao, L. Yang, R. H. Somani, C. A. Avila-Orta, and L. Zhu, "Unexpected Shish-Kebab structure in a sheared polyethylene melt," Phys. Rev. Lett. **94**(11), 117802 (2005).
[34]J. K. Hobbs, A. D. L. Humphris, and M. J. Miles, "*In-situ* atomic force microscopy of polyethylene crystallization. 1. Crystallization from an oriented backbone," Macromolecules **34**(16), 5508–5519 (2001).
[35]J. K. Hobbs, O. E. Farrance, and L. Kailas, "How atomic force microscopy has contributed to our understanding of polymer crystallization," Polymer **50**(18), 4281–4292 (2009).
[36]J. K. Hobbs and M. J. Miles, "Direct observation of polyethylene Shish-Kebab crystallization using *in-situ* atomic force microscopy," Macromolecules **34**(3), 353–355 (2001).
[37]K. Jolley and R. S. Graham, "A fast algorithm for simulating flow-induced nucleation in polymers," J. Chem. Phys. **134**(16), 164901 (2011).
[38]J. Ju, Z. Wang, F. Su, Y. Ji, H. Yang, J. Chang, S. Ali, X. Li, and L. Li, "Extensional flow-induced dynamic phase transitions in isotactic polypropylene," Macromol. Rapid Commun. **37**(17), 1441–1445 (2016).
[39]W.-G. Hu and K. Schmidt-Rohr, "Feature article," Acta Polym. **50**(2), 271–285 (1999).
[40]Z. Wang, J. Ju, L. Meng, N. Tian, J. Chang, H. Yang, Y. Ji, F. Su, and L. Li, Soft Matter **13**, 3639–3648 (2017).
[41]Z. Wang, J. Ju, J. Yang, Z. Ma, D. Liu, K. Cui, H. Yang, J. Chang, N. Huang, and L. Li, "The Non-equilibrium phase diagrams of flow-induced crystallization and melting of polyethylene," Sci. Rep. **6**, 32968 (2016).
[42]L. Li and W. H. de Jeu, "Shear-induced smectic ordering in the melt of isotactic polypropylene," Phys. Rev. Lett. **92**(7), 075506 (2004).
[43]R. G. Snyder and J. H. Schachtschneider, "Valence force calculation of the vibrational spectra of crystalline isotactic polypropylene and some deuterated polypropylenes," Spectrochim. Acta **20**(5), 853–869 (1964).
[44]G. Kumaraswamy, R. K. Verma, and J. A. Kornfield, "Novel flow apparatus for investigating shear-enhanced crystallization and structure development in semicrystalline polymers," Rev. Sci. Instrum. **70**(4), 2097–2104 (1999).
[45]W. Chen, D. Liu, and L. Li, "Multiscale characterization of semicrystalline polymeric materials by synchrotron radiation x-ray and neutron scattering," Polym. Cryst. **2**(2), 10043 (2019).
[46]T. Yan, B. Zhao, Y. Cong, Y. Fang, S. Cheng, L. Li, G. Pan, Z. Wang, X. Li, and F. Bian, "Critical strain for Shish-Kebab formation," Macromolecules **43**(2), 602–605 (2010).
[47]K. Cui, L. Meng, N. Tian, W. Zhou, Y. Liu, Z. Wang, J. He, and L. Li, "Self-acceleration of nucleation and formation of Shish in extension-induced crystallization with strain beyond fracture," Macromolecules **45**(13), 5477–5486 (2012).
[48]P. Chen, Y. Lin, J. Zhao, L. Meng, D. Wang, W. Chen, and L. Li, "Reconstructing the mechanical response of polybutadiene rubber based on micro-structural evolution in strain-temperature space: Entropic elasticity and strain-induced crystallization as the bridges," Soft Matter **16**(2), 447–455 (2020).

[49]F. E. Caputo and W. R. Burghardt, "Real-time 1-2 plane SAXS measurements of molecular orientation in sheared liquid crystalline polymers," Macromolecules **34**(19), 6684–6694 (2001).
[50]J. Baert, P. Van Puyvelde, and F. Langouche, "Flow-induced crystallization of PB-1: From the low shear rate region up to processing rates," Macromolecules **39**(26), 9215–9222 (2006).
[51]H. Janeschitz-Kriegl, E. Ratajski, and M. Stadlbauer, "Flow as an effective promotor of nucleation in polymer melts: A quantitative evaluation," Rheol. Acta **42**(4), 355–364 (2003).
[52]A. Nogales, B. S. Hsiao, R. H. Somani, S. Srinivas, A. H. Tsou, F. J. Balta-Calleja, and T. Ezquerra, "A. shear-induced crystallization of isotactic polypropylene with different molecular weight distributions: *In situ* small- and wide-angle x-ray scattering studies," Polymer **42**(12), 5247–5256 (2001).
[53]O. O. Mykhaylyk, P. Chambon, R. S. Graham, J. P. A. Fairclough, P. D. Olmsted, and A. J. Ryan, "The specific work of flow as a criterion for orientation in polymer crystallization," Macromolecules **41**(6), 1901–1904 (2008).
[54]S. Liedauer, G. Eder, H. Janeschitz-Kriegl, P. Jerschow, W. Geymayer, and E. Ingolic, "On the kinetics of shear induced crystallization in polypropylene," Int. Polym. Process. **8**(3), 236–244 (1993).
[55]R. H. Somani, B. S. Hsiao, A. Nogales, S. Srinivas, A. H. Tsou, I. Sics, F. J. Balta-Calleja, and T. A. Ezquerra, "Structure development during shear flow-induced crystallization of i-PP: *In-situ* small-angle x-ray scattering study," Macromolecules **33**(25), 9385–9394 (2000).
[56]F. Su, W. Zhou, X. Li, Y. Ji, K. Cui, Z. Qi, and L. Li, "Flow-induced precursors of isotactic polypropylene: An *in situ* time and space resolved study with synchrotron radiation scanning x-ray microdiffraction," Macromolecules **47**(13), 4408–4416 (2014).
[57]J. Chang, Z. Wang, X. Tang, F. Tian, K. Ye, and L. Li, "A portable extruder for *in situ* wide angle x-ray scattering study on multi-dimensional flow field induced crystallization of polymer," Rev. Sci. Instrum. **89**(2), 025101 (2018).
[58]X. Chen, L. Meng, W. Zhang, K. Ye, C. Xie, D. Wang, W. Chen, M. Nan, S. Wang, and L. Li, "Frustrating strain-induced crystallization of natural rubber with biaxial stretch," ACS Appl. Mater. Interfaces **11**(50), 47535–47544 (2019).
[59]H. Zhao, Q. Zhang, Z. Xia, E. Yang, M. Zhang, Y. Wang, Y. Ji, W. Chen, D. Wang, L. Meng *et al.*, "Elucidation of the relationships of structure-process-property for different ethylene/α -olefin copolymers during film blowing : An *in-situ* synchrotron radiation X-Ray scattering study," Polym. Test **85**, 106439 (2020).
[60]H. Zhao, Q. Zhang, L. Li, W. Chen, D. Wang, L. Meng, and L. Li, "Synergistic and competitive effects of temperature and flow on crystallization of polyethylene during film blowing," ACS Appl. Polym. Mater. **1**(6), 1590–1603 (2019).
[61]S. Ali, Y. Ji, Q. Zhang, H. Zhao, and W. Chen, "Preparation of polyethylene and ethylene/methacrylic acid copolymer blend films with tunable surface properties through manipulating processing parameters during film blowing," Polymers **11**(10), 1565 (2019).
[62]H. Zhao, L. Li, Q. Zhang, Z. Xia, E. Yang, Y. Wang, W. Chen, L. Meng, D. Wang, and L. Li, "Manipulation of chain entanglement and crystal networks of biodegradable poly(butylene adipate-Co-butylene terephthalate) during film blowing through the addition of a chain extender: An *in situ* synchrotron radiation x-ray scattering study," Biomacromolecules **20**(10), 3895–3907 (2019).
[63]H. Zhao, Q. Zhang, S. Ali, L. Li, F. Lv, Y. Ji, F. Su, L. Meng, and L. Li, "A real-time WAXS and SAXS study of the structural evolution of LLDPE bubble," J. Polym. Sci. Part B Polym. Phys. **56**(20), 1404–1412 (2018).
[64]R. Zhang, J. Y. Xin, Q. L. Zhang, J. J. Zhu, A. Sarmad, L. L. Fu, Z. H. Yuan, and L. L. Bin, "A universal blown film apparatus for *in situ* x-ray measurements," Chin. J. Polym. Sci. **35**(12), 1508–1516 (2017).
[65]Q. Zhang, L. Li, F. Su, Y. Ji, S. Ali, H. Zhao, L. Meng, and L. Li, "From molecular entanglement network to crystal-cross-linked network and crystal scaffold during film blowing of polyethylene: An *in situ* synchrotron radiation small- and wide-angle x-ray scattering study," Macromolecules **51**, 4350–4362 (2018).
[66]T. Yamamoto, "Molecular dynamics in fiber formation of polyethylene and large deformation of the fiber," Polymer **54**(12), 3086–3097 (2013).
[67]T. Yamamoto, "Molecular dynamics simulation of stretch-induced crystallization in polyethylene: Emergence of fiber structure and molecular network," Macromolecules **52**(4), 1695–1706 (2019).
[68]T. Yamamoto, "Molecular dynamics of crystallization in a helical polymer isotactic polypropylene from the oriented amorphous state," Macromolecules **47**(9), 3192–3202 (2014).
[69]D. A. Nicholson and G. C. Rutledge, "Molecular simulation of flow-enhanced nucleation in n-eicosane melts under steady shear and uniaxial extension," J. Chem. Phys. **145**(24), 244903 (2016).
[70]A. Keller and J. W. H. Kolnaar, "Chain extension and orientation fundamentals and relevance to processing and products," Prog. Colloid Polym. Sci. **92**, 81–102 (1993).
[71]A. Peterlin, "Hydrodynamics of linear macromolecules," Pure Appl. Chem. **12**(1–4), 563–586 (1966).
[72]P. G. De Gennes, "Coil-stretch transition of dilute flexible polymers under ultrahigh velocity gradients," J. Chem. Phys. **60**(12), 5030–5042 (1974).
[73]D. E. Smith, H. P. Babcock, and S. Chu, "Single-polymer dynamics in steady shear flow," Science **283**(80), 1724–1727 (1999).
[74]J. S. Hur, E. S. G. Shaqfeh, and R. G. Larson, "Brownian dynamics simulations of single DNA molecules in shear flow," J. Rheol. **44**(4), 713–742 (2000).
[75]J. S. Hur, E. S. G. Shaqfeh, H. P. Babcock, D. E. Smith, and S. Chu, "Dynamics of dilute and semidilute DNA solutions in the start-up of shear flow," J. Rheol. **45**(2), 421–450 (2001).
[76]H. P. Babcock, R. E. Teixeira, J. S. Hur, E. S. G. Shaqfeh, and S. Chu, "Visualization of molecular fluctuations near the critical point of the coil-stretch transition in polymer elongation," Macromolecules **36**(12), 4544–4548 (2003).
[77]C. M. Schroeder, R. E. Teixeira, E. S. G. Shaqfeh, and S. Chu, "Characteristic periodic motion of polymers in shear flow," Phys. Rev. Lett. **95**(1), 1–4 (2005).
[78]R. E. Teixeira, H. P. Babcock, E. S. G. Shaqfeh, and S. Chu, "Shear thinning and tumbling dynamics of single polymers in the flow-gradient plane," Macromolecules **38**(2), 581–592 (2005).
[79]C. M. Schroeder, R. E. Teixeira, E. S. G. Shaqfeh, and S. Chu, "Dynamics of DNA in the flow-gradient plane of steady shear flow: Observations and simulations," Macromolecules **38**(5), 1967–1978 (2005).
[80]S. Gerashchenko and V. Steinberg, "Statistics of tumbling of a single polymer molecule in shear flow," Phys. Rev. Lett. **96**(3), 5–8 (2006).
[81]R. Delgado-Buscalioni, "Cyclic motion of a grafted polymer under shear flow," Phys. Rev. Lett. **96**(8), 088303 (2006).
[82]I. S. Dalal, N. Hoda, and R. G. Larson, "Multiple regimes of deformation in shearing flow of isolated polymers," J. Rheol. **56**(2), 305–332 (2012).
[83]J. Smook and A. J. Pennings, "Elastic flow instabilities and Shish-Kebab formation during gel-spinning of ultra-high molecular weight polyethylene," J. Mater. Sci. **19**(1), 31–43 (1984).
[84]J. Smook and J. Pennings, "Influence of draw ratio on morphological and structural changes in hot-drawing of UHMW polyethylene fibres as revealed by DSC," Colloid Polym. Sci. **262**(9), 712–722 (1984).
[85]M. Seki, D. W. Thurman, J. P. Oberhauser, and J. A. Kornfield, "Shear-mediated crystallization of isotactic polypropylene: The role of long chain–long chain overlap," Macromolecules **35**(7), 2583–2594 (2002).
[86]H. Janeschitz-Kriegl and E. Ratajski, "Kinetics of polymer crystallization under processing conditions: Transformation of dormant nuclei by the action of flow," Polymer **46**(11), 3856–3870 (2005).
[87]H. Janeschitz-Kriegl, "Some remarks on flow induced crystallization in polymer melts," J. Rheol. **57**(4), 1057–1064 (2013).
[88]S. Liedauer, G. Eder, and H. Janeschitz-Kriegl, "On the limitations of shear induced crystallization in polypropylene melts," Int. Polym. Process **10**(3), 243–250 (1995).
[89]K. Cui, D. Liu, Y. Ji, N. Huang, Z. Ma, Z. Wang, F. Lv, H. Yang, and L. Li, "Nonequilibrium nature of flow-induced nucleation in isotactic polypropylene," Macromolecules **48**(3), 694–699 (2015).
[90]L. Li and W. H. De Jeu, "Shear-induced smectic ordering as a precursor of crystallization in isotactic polypropylene," Macromolecules **36**(13), 4862–4867 (2003).

[91]L. Yang, R. H. Somani, I. Sics, B. S. Hsiao, R. Kolb, H. Fruitwala, and C. Ong, "Shear-induced crystallization precursor studies in model polyethylene blends by *in-situ* Rheo-SAXS and Rheo-WAXD," Macromolecules **37**(13), 4845–4859 (2004).
[92]R. H. Somani, L. Yang, B. S. Hsiao, P. K. Agarwal, H. A. Fruitwala, and A. H. Tsou, "Shear-induced precursor structures in isotactic polypropylene melt by *in-situ* Rheo-SAXS and Rheo-WAXD studies," Macromolecules **35**(24), 9096–9104 (2002).
[93]P. K. Agarwal, R. H. Somani, W. Weng, A. Mehta, L. Yang, S. Ran, L. Liu, and B. S. Hsiao, "Shear-induced crystallization in novel long chain branched polypropylenes by *in situ* Rheo-SAXS and -WAXD," Macromolecules **36**(14), 5226–5235 (2003).
[94]R. H. Somani, L. Yang, B. S. Hsiao, T. Sun, N. V. Pogodina, and A. Lustiger, "Shear-induced molecular orientation and crystallization in isotactic polypropylene: Effects of the deformation rate and strain," Macromolecules **38**(4), 1244–1255 (2005).
[95]N. V. Pogodina, S. K. Siddiquee, J. W. Van Egmond, and H. H. Winter, "Correlation of rheology and light scattering in isotactic polypropylene during early stages of crystallization," Macromolecules **32**(4), 1167–1174 (1999).
[96]N. V. Pogodina and H. H. Winter, "Polypropylene crystallization as a physical gelation process," Macromolecules **31**(23), 8164–8172 (1998).
[97]N. V. Pogodina, V. P. Lavrenko, S. Srinivas, and H. H. Winter, "Rheology and structure of isotactic polypropylene near the gel point: Quiescent and shear-induced crystallization," Polymer **42**(21), 9031–9043 (2001).
[98]N. V. Pogodina, H. H. Winter, and S. Srinivas, "Strain effects on physical gelation of crystallizing isotactic polypropylene," J. Polym. Sci. B: Polym. Phys. **37**(24), 3512–3519 (1999).
[99]G. Kumaraswamy, R. K. Verma, A. M. Issaian, P. Wang, J. A. Kornfield, F. Yeh, B. S. Hsiao, and R. H. Olley, "Shear-enhanced crystallization in isotactic polypropylene part 2. Analysis of the formation of the oriented "skin," Polymer **41**(25), 8931–8940 (2000).
[100]G. Kumaraswamy, J. A. Kornfield, F. Yeh, and B. S. Hsiao, "Shear-enhanced crystallization in isotactic polypropylene. 3. Evidence for a kinetic pathway to nucleation," Macromolecules **35**(5), 1762–1769 (2002).
[101]G. Kumaraswamy, A. M. Issaian, and J. A. Kornfield, "Shear-enhanced crystallization in isotactic polypropylene. 1. Correspondence between *in situ* rheo-optics and *ex situ* structure determination," Macromolecules **32**(22), 7537–7547 (1999).
[102]Z. Wang, Z. Ma, and L. Li, "Flow-induced crystallization of polymers: Molecular and thermodynamic considerations," Macromolecules **49**(5), 1505–1517 (2016).
[103]D. Liu, N. Tian, N. Huang, K. Cui, Z. Wang, T. Hu, H. Yang, X. Li, and L. Li, "Extension-induced nucleation under near-equilibrium conditions: The mechanism on the transition from point nucleus to Shish," Macromolecules **47**(19), 6813–6823 (2014).
[104]H. Yang, D. Liu, J. Ju, J. Li, Z. Wang, G. Yan, Y. Ji, W. Zhang, G. Sun, and L. Li, "Chain deformation on the formation of Shish nuclei under extension flow: An *in situ* SANS and SAXS study," Macromolecules **49**(23), 9080–9088 (2016).
[105]Y. Liang, Y. Guo, E. Wang, and M. Cakmak, "Details of molecular organization during strain-induced crystallization in natural rubber/clay systems as revealed by real-time mechano-optical behavior," Macromolecules **48**(7), 2299–2304 (2015).
[106]B. H. Zimm and J. K. Bragg, "Theory of the phase transition between helix and random coil in polypeptide chains," J. Chem. Phys. **31**(2), 526–535 (1959).
[107]T. Shimada, M. Doi, and K. Okano, "Concentration fluctuation of stiff polymers. III. Spinodal decomposition," J. Chem. Phys. **88**(11), 7181–7186 (1988).
[108]M. Doi, T. Shimada, and K. Okano, "Concentration fluctuation of stiff polymers. II. Dynamical structure factor of rod-like polymers in the isotropic phase," J. Chem. Phys. **88**(6), 4070–4075 (1988).
[109]C. K. Chai, N. M. Dixon, D. L. Gerrard, and W. Reed, "Rheo-Raman studies of polyethylene melts," Polymer **36**(3), 661–663 (1995).
[110]Y. Cong, Z. Hong, Z. Qi, W. Zhou, H. Li, H. Liu, W. Chen, X. Wang, and L. Li, "Conformational ordering in growing spherulites of isotactic polypropylene," Macromolecules **43**(23), 9859–9864 (2010).
[111]Y. Cong, Z. Hong, W. Zhou, W. Chen, F. Su, H. Li, X. Li, K. Yang, X. Yu, Z. Qi *et al.*, "Conformational ordering on the growth front of isotactic polypropylene spherulite," Macromolecules **45**(21), 8674–8680 (2012).
[112]X. Zhu, D. Yan, and Y. Fang, "*In situ* FTIR spectroscopic study of the conformational change of isotactic polypropylene during the crystallization process," J. Phys. Chem. B **105**(50), 12461–12463 (2001).
[113]H. An, B. Zhao, M. Zhe, C. Shao, X. Wang, Y. Fang, A. Li, and Z. Li, "Shear-induced conformational ordering in the melt of isotactic polypropylene," Macromolecules **40**(14), 4740–4743 (2007).
[114]F. Su, Y. Ji, L. Meng, Z. Wang, Z. Qi, J. Chang, J. Ju, and L. Li, "Coupling of multiscale orderings during flow-induced crystallization of isotactic polypropylene," Macromolecules **50**(5), 1991–1997 (2017).
[115]C. Xie, X. Tang, J. Yang, T. Xu, F. Tian, and L. Li, "Stretch-induced coil-helix transition in isotactic polypropylene: A molecular dynamics simulation," Macromolecules **51**(11), 3994–4002 (2018).
[116]D. Turnbull and J. C. Fisher, "Rate of nucleation in condensed systems," J. Chem. Phys. **17**(1), 71–73 (1949).
[117]A. Sauter, F. Roosen-Runge, F. Zhang, G. Lotze, A. Feoktystov, R. M. J. Jacobs, and F. Schreiber, "On the question of two-step nucleation in protein crystallization," Faraday Discuss. **179**, 41–58 (2015).
[118]M. Anwar, J. T. Berryman, and T. Schilling, "Crystal nucleation mechanism in melts of short polymer chains under quiescent conditions and under shear flow," J. Chem. Phys. **141**(12), 124910 (2014).
[119]X. Tang, J. Yang, T. Xu, F. Tian, C. Xie, and L. Li, "Local structure order assisted two-step crystal nucleation in polyethylene," Phys. Rev. Mater. **1**(7), 073401 (2017).
[120]X. Tang, J. Yang, F. Tian, T. Xu, C. Xie, W. Chen, and L. Li, "Flow-induced density fluctuation assisted nucleation in polyethylene," J. Chem. Phys. **149**(22), 224901 (2018).
[121]H. An, X. Li, Y. Geng, Y. Wang, X. Wang, A. Li, Z. Li, and C. Yang, "Shear-induced conformational ordering, relaxation, and crystallization of isotactic polypropylene," J. Phys. Chem. B **112**(39), 12256–12262 (2008).
[122]Y. Geng, G. Wang, Y. Cong, L. Bai, L. Li, and C. Yang, "Shear-induced nucleation and growth of long helices in supercooled isotactic polypropylene," Macromolecules **42**(13), 4751–4757 (2009).
[123]R. H. Boyd, R. H. Gee, J. Han, and Y. Jin, "Conformational dynamics in bulk polyethylene: A molecular dynamics simulation study," J. Chem. Phys. **101**(1), 788–797 (1994).
[124]D. Hossain, M. A. Tschopp, D. K. Ward, J. L. Bouvard, P. Wang, and M. F. Horstemeyer, "Molecular dynamics simulations of deformation mechanisms of amorphous polyethylene," Polymer **51**(25), 6071–6083 (2010).
[125]J. Yang, X. Tang, Z. Wang, T. Xu, F. Tian, Y. Ji, and L. Li, "Coupling between intra- and inter-chain orderings in flow-induced crystallization of polyethylene: A non-equilibrium molecular dynamics simulation study," J. Chem. Phys. **146**(1), 014901 (2017).
[126]C. Liu and M. Muthukumar, "Langevin dynamics simulations of early-stage polymer nucleation and crystallization," J. Chem. Phys. **109**(6), 2536–2542 (1998).
[127]M. Muthukumar, M. J. W. Povey, S. Edwards, and A. H. Windle, "Molecular modelling of nucleation in polymers," Philos. Trans. R. Soc. A Math. Phys. Eng. Sci. **361**(1804), 539–556 (2003).
[128]D. Petera and M. Muthukumar, "Brownian dynamics simulation of bead-rod chains under shear with hydrodynamic interaction," J. Chem. Phys. **111**(16), 7614–7623 (1999).
[129]M. S. Lavine, N. Waheed, and G. C. Rutledge, "Molecular dynamics simulation of orientation and crystallization of polyethylene during uniaxial extension," Polymer **44**(5), 1771–1779 (2003).
[130]M. J. Ko, N. Waheed, M. S. Lavine, and G. C. Rutledge, "Characterization of polyethylene crystallization from an oriented melt by molecular dynamics simulation," J. Chem. Phys. **121**(6), 2823–2832 (2004).
[131]C. Luo and J. U. Sommer, "Growth pathway and precursor states in single lamellar crystallization: MD simulations," Macromolecules **44**(6), 1523–1529 (2011).

[132]M. Wittkop, J.-U. Sommer, S. Kreitmeier, and D. Göritz, "Monte Carlo simulations of a single polymer chain under an external force in two and three dimensions," Phys. Rev. E **49**(6), 5472–5476 (1994).
[133]J. U. Sommer and C. Luo, "Molecular dynamics simulations of semicrystalline polymers: Crystallization, melting, and reorganization," J. Polym. Sci. Part B Polym. Phys. **48**(21), 2222–2232 (2010).
[134]X. Guan, J. Wang, and W. Hu, "Monte Carlo simulation of strain-enhanced stereocomplex polymer crystallization," J. Phys. Chem. B **122**(48), 10928–10933 (2018).
[135]Y. Nie, Y. Zhao, G. Matsuba, and W. Hu, "Shish-Kebab crystallites initiated by shear fracture in bulk polymers," Macromolecules **51**(2), 480–487 (2018).
[136]L. Zha, Y. Wu, and W. Hu, "Multicomponent thermodynamics of strain-induced polymer crystallization," J. Phys. Chem. B **120**(27), 6890–6896 (2016).
[137]I. Ogura and T. Yamamoto, "Molecular dynamics simulation of large deformation in an amorphous polymer," Polymer **36**(7), 1375–1381 (1995).
[138]T. Yamamoto, "Molecular dynamics simulation of polymer ordering. II. Crystallization from the melt," J. Chem. Phys. **115**(18), 8675–8680 (2001).
[139]A. Koyama, T. Yamamoto, K. Fukao, and Y. Miyamoto, "Molecular dynamics studies on polymer crystallization from a stretched amorphous state," J. Macromol. Sci. B **42**(3–4), 821–831 (2003).
[140]P. J. Flory, "Thermodynamics of crystallization in high polymers. I. Crystallization induced by stretching," J. Chem. Phys. **15**(6), 397–408 (1947).
[141]R. Becker and W. Döring, "Kinetische Behandlung Der Keimbildung in Übersättigten Dämpfen," Ann. Phys. **416**(8), 719–752 (1935).
[142]P. J. Flory, "Thermodynamics of crystallization in high polymers. IV. A theory of crystalline states and fusion in polymers, copolymers, and their mixtures with diluents," J. Chem. Phys. **17**(3), 223–240 (1949).
[143]M. Doi and S. F. Edwards, "Dynamics of concentrated polymer systems. part 2—Molecular motion under flow," J. Chem. Soc. Faraday Trans. **74**, 1802–1817 (1978).
[144]S. Coppola, N. Grizzuti, and P. L. Maffettone, "Microrheological modeling of flow-induced crystallization," Macromolecules **34**(14), 5030–5036 (2001).
[145]N. Tian, W. Zhou, K. Cui, Y. Liu, Y. Fang, X. Wang, L. Liu, and L. Li, "Extension flow induced crystallization of poly(ethylene oxide)," Macromolecules **44**(19), 7704–7712 (2011).
[146]J. J. D. Yoreo, P. U. P. A. Gilbert, N. A. J. M. Sommerdijk, R. L. Penn, S. Whitelam, D. Joester, H. Zhang, J. D. Rimer, A. Navrotsky, J. F. Banfield *et al.*, "Crystallization by particle attachment in synthetic, biogenic, and geologic environments," Science **349**(80), aaa6760 (2015).
[147]A. E. S. Van Driessche, L. G. Benning, J. D. Rodriguez-Blanco, M. Ossorio, P. Bots, and J. M. Garcia-Ruiz, "The role and implications of Bassanite as a stable precursor phase to gypsum precipitation," Science **336**(80), 69–72 (2012).
[148]Y. Politi, T. Arad, E. Klein, S. Weiner, and L. Addadi, "Sea urchin spine calcite forms via a transient amorphous calcium carbonate phase," Science **306**(80), 1161–1164 (2004).
[149]W. Chen, Y. Wu, B. Zhang, Y. Wang, F. Li, and Z. Qi, "Retardation behavior of hydration of calcium sulfate hemihydrate (Bassanite) induced by sodium trimetaphosphate (STMP)," CrystEngComm **20**(12), 1662–1668 (2018).
[150]P. A. Fang, J. F. Conway, H. C. Margolis, J. P. Simmer, and E. Beniash, "Hierarchical self-assembly of amelogenin and the regulation of biomineralization at the nanoscale," Proc. Natl. Acad. Sci. U.S.A. **108**(34), 14097–14102 (2011).
[151]D. Li, M. H. Nielsen, J. R. I. Lee, C. Frandsen, J. F. Banfield, and J. J. De Yoreo, "Direction-specific interactions control crystal growth by oriented attachment," Science **336**(80), 1014–1018 (2012).
[152]K. J. Johnson, L. Wiegart, A. C. Abbott, E. B. Johnson, J. W. Baur, and H. Koerner, "In operando monitoring of dynamic recovery in 3D-printed thermoset nanocomposites by XPCS," Langmuir **35**(26), 8758–8768 (2019).